

# Bending of the concentration discharge relationship can inform about in-stream nitrate removal

Joni Dehaspe<sup>1,2</sup>, Fanny Sarrazin<sup>3</sup>, Rohini Kumar<sup>3</sup>, Jan H. Fleckenstein<sup>1,4</sup> and Andreas Musolff<sup>1</sup>

<sup>1</sup>Department of Hydrogeology, UFZ- Helmholtz-Centre for Environmental Research, 04318 Leipzig, Germany

5 <sup>2</sup>Unit Environmental Modeling, Flemish Institute for Technological Research NV- VITO, Boeretang 200, 2400, Mol, Belgium

<sup>3</sup>Department Computational Hydrosystems, UFZ - Helmholtz-Centre for Environmental Research, 04318 Leipzig, Germany

<sup>4</sup>Bayreuth Center of Ecology and Environmental Research, University of Bayreuth, 95440 Bayreuth, Germany

*Correspondence to:* Joni Dehaspe (joni.dehaspe@ufz.de)

**Abstract.** Nitrate ( $\text{NO}_3^-$ ) excess in rivers harms aquatic ecosystems and can induce detrimental algae growths in coastal areas. Riverine  $\text{NO}_3^-$  uptake is a crucial element of the catchment scale nitrogen balance and can be measured at small spatiotemporal scales while at the scale of entire river networks, uptake measurements are rarely available. Concurrent, low frequency  $\text{NO}_3^-$  concentration and stream flow (Q) observations at a basin outlet, however, are commonly monitored and can be analyzed in terms of concentration discharge (C-Q) relationships. Previous studies suggest that steeper positive  $\log(\text{C})$ - $\log(\text{Q})$  slopes under low flow conditions (than under high flows) are linked to biological  $\text{NO}_3^-$  uptake, creating a bent rather than linear  $\log(\text{C})$ - $\log(\text{Q})$  relationship. Here we explore if network scale  $\text{NO}_3^-$  uptake creates bent  $\log(\text{C})$ - $\log(\text{Q})$  relationships and when in turn uptake can be quantified from observed low frequency C-Q data. To this end we apply a parsimonious mass balance based river network uptake model in 13 mesoscale German catchments (21-1450 km<sup>2</sup>) and explore the linkages between  $\log(\text{C})$ - $\log(\text{Q})$  bending and different model-parameter combinations. The modelling results show that uptake and transport in the river network can create bent  $\log(\text{C})$ - $\log(\text{Q})$  relationships at the basin outlet from  $\log$ - $\log$  linear C-Q relationships describing the  $\text{NO}_3^-$  land to stream transfer. We find that within the chosen parameter range the bending is mainly shaped by geomorphological parameters that control the channel reactive surface area rather than by the biological uptake velocity itself. Further we show that in this exploratory modelling environment, bending is positively correlated to percentage  $\text{NO}_3^-$  load removed in the network ( $L_{r,perc}$ ) but that network wide flow velocities should be taken into account when interpreting  $\log(\text{C})$ - $\log(\text{Q})$  bending. Classification trees, finally, can successfully predict classes of low (~4 %), intermediate (~32 %) and high (~68 %)  $L_{r,perc}$  using information on water velocity and  $\log(\text{C})$ - $\log(\text{Q})$  bending. These results can help to identify stream networks that efficiently attenuate  $\text{NO}_3^-$  loads based on low frequency  $\text{NO}_3^-$  and Q observations and generally show the importance of the channel geomorphology on the emerging  $\log(\text{C})$ - $\log(\text{Q})$  bending at network scales.

## 1 Introduction

Transport and transformation of nitrate ( $\text{NO}_3^-$ ) in river networks are major controls of downstream exports to receiving lakes, reservoirs and coastal systems (Alexander et al., 2000; Billen et al., 1991; Peterson et al., 2001; Seitzinger et al., 2002; Seybold

and McGlynn, 2018). Increased  $\text{NO}_3^-$  concentrations in surface waters can induce detrimental algae growths (Beusen et al., 2016; Canfield et al., 2010; Galloway et al., 1995), compromise river ecosystem health and jeopardize drinking water supplies. Since the beginning of the 20<sup>th</sup> century, human activities such as agricultural expansion and fossil fuel burning have mobilized additional reactive nitrogen (N), initiating and later exacerbating this problem (Seitzinger et al., 2002). In arable landscapes, which include large parts of Europe, the efficient management of aquatic  $\text{NO}_3^-$  at network scales is complicated by the spatiotemporal variability of loading patterns and hydrologic regimes as well as the lack of understanding of nutrient pathways, connected transit times and removal processes from input to export. Nevertheless, nitrate concentration and load variability can be predicted at catchment scales when relying on detailed process understanding regarding transport and biogeochemical processing (Alexander et al., 2009; Schlesinger et al., 2006; Wollheim et al., 2008). Moving beyond small scale variability and characterizing nitrate processing at the catchment scale however remains a challenge (McDonnell et al., 2007; Li et al., 2020).

Within river reaches and streams, reactive solutes like  $\text{NO}_3^-$  are affected by complex interactions of physical, biological and chemical processes. Physical transport is driven by local discharge and channel geomorphology and dictates the  $\text{NO}_3^-$  residence time in a reach, thus influencing the timescales at which biogeochemical processing can take place (Kirchner et al., 2000; Runkel and Bencala, 1995; Zarnetske et al., 2011).  $\text{NO}_3^-$  is removed and transformed by denitrifying bacteria in the anoxic river sediment (Birgand et al., 2007; Peterson et al., 2001), ammonified or retained through assimilation processes in the oxic or anoxic river compartments by bacteria, fungi and primary producers such as algae and macrophytes, potentially entering higher trophic levels. In the latter case, N in the form of DON (dissolved organic nitrogen) and more commonly DIN (dissolved inorganic nitrogen), together with phosphorus (P) may be released to the water column later on (Durand et al., 2011; Vanni, 2002; Vanni and McIntyre, 2016). The nutrient spiraling model (Newbold et al., 1981; Stream Solute Workshop, 1990) that formally describes these processes has been used to quantify and compare  $\text{NO}_3^-$  transport and uptake (the net result of all removal and release processes) in river reaches (Peterson et al., 2001; Mulholland et al., 2008; Hall et al., 2009) and stream networks (Ensign et al., 2006; Doyle, 2005; Marce and Armengol, 2009). Quantifying in situ  $\text{NO}_3^-$  uptake is labor intensive and may involve local nutrient additions, potentially altering the ambient uptake rate (Hensley et al., 2014; Mulholland and Tank, 2002). Other methods require high frequency measurements (Jarvie et al., 2018; Kunz et al., 2017) that are mostly limited to small spatial scales (i.e. reach scale) and can vary considerably between measuring points (Boyer et al., 2006). At the scale of entire river networks contrarily, uptake measurements are rarely available (but see Wollheim et al., 2017; Hansen et al 2018) and models are applied instead to predict spatiotemporal uptake patterns (Boyer et al., 2006; Yang et al., 2018). These models account for the spatial configuration of the stream network, an important aspect for stream biogeochemistry that is often ignored in small scale experimental approaches (Fisher et al., 2004). Spatially distributed models however, require calibration of uncertain spatiotemporal parameters and may not reflect the essential features of the system despite fitting observed data well (Klemes, 1986).

River networks link terrestrial source zones to coastal areas and integrate biogeochemical and hydrological catchment functions across scales (Bouwman et al., 2012; Helton et al., 2018). Small streams (usually headwaters) are known to influence the export signal disproportionately because of their overall (high) contribution to total stream length and effective  $\text{NO}_3^-$  removal capacity (Alexander et al., 2000; Horton, 1945), explained by high sediment surface to water volume ratios. Generally, high removal efficiencies have been reported for river network areas with lower specific discharges (Hall et al., 2009; Hensley et al., 2014), under favorable circumstances such as high light availability, heavy in-stream vegetation (Hensley et al., 2014; Rode et al., 2016) and for streams with a high capacity for lateral and hyporheic exchange (Gomez-Velez et al., 2015; Kiel and Cardenas, 2014). The scaling of in-stream uptake processes beyond the river reach has been approached by combined experimental-modelling studies with defined explicit scaling relationships (e.g. Basu et al., 2011; Aguilera et al., 2013; Bertuzzo et al., 2017; Lindgren and Destouni, 2004) and theoretical frameworks explaining how the river network capacity regulates solute export (e.g. Wollheim et al., 2018). Abbott et al. (2018) shows how spatially heterogeneous patterns of water chemistry stabilize while the temporal variability of nutrient concentrations persists when moving downstream, facilitating the temporal scaling of headwater measurements. Nevertheless, insights into linking the interplay of nitrate removal processes at the network scale to downstream export patterns in space and time are largely missing.

Concentrations (C) for in-stream solutes such as carbon, major ions, particulates and nutrients are commonly monitored concurrently with discharge (Q) at the basin outlet. C-Q relationships integrate the effect of biogeochemical and hydrological processes within the catchment and have mainly been discussed in terms of land-stream transfer and source configuration in catchments as well as subsurface retention processes (Godsey et al., 2009; Musolff et al., 2017, Bierzoza et al., 2018). The shape of long term (multiple years) C-Q relationships in the log-log space is typically described by the slope of a linear regression model (Godsey et al., 2009). Here, three archetypes have been distinguished; (i) a positive  $\log(\text{C})$ - $\log(\text{Q})$  slope, indicating enrichment, occurs when an increasing discharge additionally mobilizes solutes, (ii) a negative C-Q slope or dilution pattern is commonly linked with source limitations and (iii) a neutral or chemostatic slope implies low variability in in-stream concentrations across a high range of discharges, a pattern observed for example for solutes derived from weathering bedrock (Ameli et al., 2017; Godsey et al., 2009). The potential information loss associated with linear and monotonic  $\text{NO}_3^-$   $\log(\text{C})$ - $\log(\text{Q})$  analysis was addressed by Moatar et al. (2017) and Minaudo et al. (2019) for more than 200 French catchments and by Diamond and Cohen (2018) for 44 rivers in Florida, USA. These studies identified distinct linear low-flow and high-flow  $\text{NO}_3^-$   $\log(\text{C})$ - $\log(\text{Q})$  regression slopes for a majority of the cases, using low frequency monitoring data. Moatar et al. (2017) found that stronger positive slopes under low flow conditions correlate positively with chlorophyll-a concentrations (associated with biological processes) and attributed this condition to biological  $\text{NO}_3^-$  concentration mediation in the stream. This is consistent with the findings of Hall et al. (2009) and Hensley et al. (2014) among others that in-stream uptake is more efficient under low-flow than under high-flow. Furthermore, Wollheim et al. (2017) illustrates non-linear  $\text{NO}_3^-$  C-Q relationships conceptually for storm flow dynamics in a river network, showing high retention capacities in the headwater catchments that decrease under increasing flows, changing the slope of C-Q relationships from dilution to enrichment. Based on these studies we hypothesize

that the magnitude (or efficiency) of in-stream  $\text{NO}_3^-$  uptake is encoded within observed C-Q relationships, and their analysis therefore can improve our understanding of in-stream uptake processes through providing an alternative to elaborate field and modelling work aimed at quantifying  $\text{NO}_3^-$  removal in stream networks. Low frequency  $\text{NO}_3^-$  observations are widely available (e.g. biweekly to monthly grab sampling, Ebeling et al., 2020 rev; Minaudo et al., 2019; Moatar et al., 2017) but if and how this data can be utilized to characterize catchment scale in-stream processing has yet to be investigated.

In this paper, it is postulated that network-scale uptake effects can be inferred from the degree of non-linearity or the amount of bending of low-frequency, multi-annual concentration (C) and discharge (Q) observations. To test this hypothesis, we apply a parsimonious river network model (similar to Bertuzzo et al., 2017; Helton et al., 2018; Helton et al., 2010; Mulholland et al., 2008) in 13 German catchments to explore the catchment scale transport and uptake processes that influence downstream  $\log(\text{C})$ - $\log(\text{Q})$  patterns. The specific objectives are to (i) introduce the maximum curvature ( $Curv_{max}$ ) as a robust metric to quantify bending of low frequency C-Q time series in the log-log space; (ii) explore the sensitivity of  $Curv_{max}$  to hydrological and in-stream biogeochemical parameters (e.g. channel shape, water velocity and biological  $\text{NO}_3^-$  uptake velocity); (iii) explore how C-Q bending is linked to network scale in-stream uptake; (iv) provide guidelines if and under what circumstances the C-Q bending can offer conclusive information on effective in-stream uptake. In this proof of concept exploratory study, we demonstrate how (existing) low-frequency monitoring data can be effectively utilized to quantify nitrate uptake in river networks and show how small scale uptake processes shape emerging patterns at catchment scales.

## 2 Methods

### 2.1 Maximum curvature - $Curv_{max}$

The shape of  $\log(\text{C})$ - $\log(\text{Q})$  relationships are often described as linear (Bieroza et al., 2018; Godsey et al., 2009; Musolff et al., 2017) or segmented linear (Meybeck and Moatar, 2012; Moatar et al., 2017; Marinos et al., 2020), implying a limit on the possible  $\log(\text{C})$ - $\log(\text{Q})$  shapes (Tunqui Neira et al., 2020) and setting assumptions such as ‘fixed breaking points’. Here, we introduce the concept of maximum curvature ( $Curv_{max}$ ) to quantify rather than describe the shape of "broken-stick"  $\log(\text{C})$ - $\log(\text{Q})$  relationships, without the assumption of a fixed form. In a strict geometrical sense the curvature ( $-\infty$ ;  $+\infty$ ) is the instantaneous rate of change of direction of a point that moves on a curve. A straight line for example has a curvature of zero and a large circle has a lower absolute curvature than a small circle (Pressley, 2001). Here,  $Curv_{max}$  identifies the magnitude and direction of the  $\log(\text{C})$ - $\log(\text{Q})$  section with the largest instantaneous change. To calculate  $Curv_{max}$  for an observed (noisy)  $\log(\text{C})$ - $\log(\text{Q})$  relationship, a smoothed spline,  $f$ , is iteratively fitted with increasing degrees of freedom (df) to capture the general  $\log(\text{C})$ - $\log(\text{Q})$  shape accurately but avoid overfitting (Fig. B1). Initially,  $df = 3$  and the  $\log(\text{Q})$  region of the largest instantaneous change is identified as  $Q_m \pm 0.05$  with  $Q_m = \underset{\log Q}{\text{argmax}} |f''|$ . Then,  $df$  is increased until, at  $df=i$ , the  $\log(\text{Q})$  corresponding to the largest instantaneous change is not within the initial  $Q_m$  region anymore. Consequently,  $Curv_{max}$  is

calculated for a smoothed spline fit,  $f$ , with  $df = i-1$  as  $\begin{cases} \max_{\log Q} f'' \text{ if } \left| \max_{\log Q} f'' \right| \geq \left| \min_{\log Q} f'' \right| \\ \min_{\log Q} f'' \text{ if } \left| \max_{\log Q} f'' \right| < \left| \min_{\log Q} f'' \right| \end{cases}$ . The  $Curv_{max}$  metric, computed for a

130  $\log(C)$ - $\log(Q)$  relationship could be considered as a complementary metric to the slope of the linear regression model (Godsey et al., 2009) and could serve as an alternative for segmented linear regression fits (Meybeck and Moatar, 2012; Moatar et al., 2017; Marinos et al., 2020) (Fig. S1 in the Supporting Information) as it quantifies the degree of non-linearity as the amount of bending.

135 We assume here that a multi-annual (6 to 15 years) low frequency (biweekly to monthly) C-Q relationship without temporal (significant) trends in a given station has one  $Curv_{max}$ . To verify this assumption in a realistic setting,  $Curv_{max}$  was computed for observed nitrate (C) and Q data (1995-2010) of French water quality stations with biweekly to monthly sampling frequencies (Dupas et al., 2019). Following the removal of C outliers (falling outside of  $\mu \pm 3.5\sigma$  in the log space, with  $\mu$  and  $\sigma$  representing the sample mean and standard deviation, respectively) 444 stations were selected that satisfy the following four

140 criteria: (i) the station should have at least 70 coupled C and Q observations (the maximum number of samples within one station was 402 ); (ii) a minimum of 6 years of data are represented; (iii) there is no bias in the intra annual distribution of the data (i.e. never less than 10 % of the C-Q observations in one season; Fig. S2); and (iv) the station C observations had no significant temporal trends (Mann Kendall test, p-value > 0.05) (Ebeling et al., 2021). We then assessed the robustness of  $Curv_{max}$  to the low frequency C-Q observations in a time series by selecting different subsamples of C-Q data from the entire

145 available time series for a given station. More specifically, 100 random time series subsamples (each with a minimum length of 70) without replacement but with overlap were taken for each station, with the subsamples passing the four criteria above, and  $Curv_{max}$  was calculated for each subsampled time series. On average, the subsamples represented nearly 80% of the complete time series for a station.

## 150 2.2 Network Model

In this work an explorative grid based (100 m x 100 m) mass balance network model (comparable to Bertuzzo et al., 2017; Helton et al., 2018; Helton et al., 2010; Mulholland et al., 2008 and conceptually shown in Fig. B2) was used to simulate in-stream nitrate transport and biological removal on a daily basis. The model was developed in R (R Core Team, 2013).

### 2.2.1 Stream network and hydrological properties

155 Following Bertuzzo et al. (2017) and Helton et al. (2018), each river network node (i.e. grid cell)  $i$  ( $1 \leq i \leq N$ ) has a drainage area  $A_i$  [m<sup>2</sup>] that is calculated as the sum of the total upstream drainage area  $\sum_j W_{ji} A_j$  [m<sup>2</sup>] and the direct drainage area  $a_i$  [m<sup>2</sup>] (e.g. laterally contributing drainage area) to grid cell  $i$  (Eq. (1)):

$$A_i = \underbrace{\sum_j W_{ji} A_j}_{\text{Upstream Drainage Areas}} + \underbrace{a_j}_{\text{Direct Drainage Area}} \quad (1)$$

where  $W_{ji}$  [-] is an element in the connectivity matrix  $W$  ( $N \times N$ ) such that  $W_{ji} = 1$  if  $j$  is directly neighboring and flowing into  $i$  and  $W_{ji} = 0$  otherwise.  $A_j$  [ $\text{m}^2$ ] is the total drainage area to node  $j$ .

It is the spatially varying contribution of the total upstream and direct drainage area to each river network node that creates the spatial variability in the river network. The temporal variability in the river network is driven by the time varying but spatially homogeneous specific discharge  $Q_{t.sp}$  [ $\text{m}^3 \text{s}^{-1}$ ], calculated as the ratio of the daily discharge at the catchment outlet and the total number of catchment grid cells. The total local discharge  $Q_i$  [ $\text{m}^3 \text{s}^{-1}$ ] at a given grid cell  $i$  is thus proportional to the total drainage area at that grid cell,  $A_i$ , (following Bergstrom et al., 2016 and Bertuzzo et al., 2017) (Eq. (2)). It is  $Q_i$  which in turn dictates the downstream and at-a-station hydraulic geometry relationships of river geomorphic parameters channel width,  $w_i$  [m], and average channel depth,  $d_i$  [m] (Leopold and Maddock, 1953) (Eq. (2.1) and Eq. (2.2)). The local velocity in a grid cell  $v_i$  [ $\text{m s}^{-1}$ ] is calculated according to Eq. (2.3) and the corresponding travel time,  $T_i$  [days] is computed in Eq. (2.4):

$$Q_i = Q_{t.sp} * A_i \quad (2)$$

$$w_i = K_w * Q_i^{a_w} \quad (2.1)$$

$$d_i = K_d * Q_i^{a_d} \quad (2.2)$$

$$v_i = \frac{Q_i}{w_i * d_i} \quad (2.3)$$

$$T_i = \frac{l_i}{v_i} \quad (2.4)$$

where the flow length through a grid cell  $i$ ,  $l_i$  [m], equals 100 or  $100\sqrt{2}$  m for horizontal/vertical or diagonal flow directions, respectively. Parameters  $a_w$  [-] and  $K_w$  [-] are the respective exponent and coefficient parameters in the river width-discharge relationship (Eq. (2.1)); while  $a_d$  [-] and  $K_d$  [-] compose the exponent and coefficient parameters of the depth-discharge relationship (Eq. (2.2)), respectively. The ratio of  $a_d$  to  $a_w$  corresponds to a parameter  $r$  [-]  $\in \mathbb{R}^+$  which prescribes the cross section geometry relation such that a triangular channel cross section is represented by  $r = 1$ , a parabolic channel cross section by  $r = 2$  and channel cross sections with progressively flatter bottoms and steeper banks by increasing values of  $r$  (Dingman, 2007). The width-discharge relation in Eq. (2.1) is conceptually illustrated in Fig. B3 for two sets of  $a_w$  and  $K_w$ , where a low  $a_w$  corresponds to the width of a channel that does not change much with varying discharge, while a high  $a_w$  can result in highly varying channel widths.

### 2.2.2 Nitrate uptake

Similar to Eq. (1) the incoming load,  $L_{in,i}$  [ $\text{mg s}^{-1}$ ], to a river network grid cell  $i$  is composed as the sum of upstream load contributions  $L_{in.up,i}$  [ $\text{mg s}^{-1}$ ] and direct land to stream loading  $L_{in.ls,i}$  [ $\text{mg s}^{-1}$ ], given that  $L = CQ$  (Eq. (3)). The contribution of direct land to stream loading concentration can be expressed as a power law (Musolff et al. 2017) with the exponent  $b$  [-],

the slope in the log(C)-log(Q) relationship that is an indicator of the C-Q archetype (Godsey et al., 2009) and coefficient  $c$  [-]. Here,  $b$  is assumed to be constant over the seasons, which considers that  $\text{NO}_3^-$  loading is transport limited rather than source limited as explicitly shown for agricultural catchments (Basu et al., 2011; Winter et al., 2021). Following Jawitz and Mitchell (2011), the coefficient  $c$  is calculated to yield the long-term mean in-stream input concentration  $C_{mean}$  [ $\text{mg L}^{-1}$ ] (Eq. (A1)). Additional  $\text{NO}_3^-$  sources such as the load resulting from  $\text{NO}_3^-$  release within the stream network and point sources are not considered here (similar to Bertuzzo et al., 2017; Wollheim et al., 2006). This assumption is supported by large scale assessments in France (Moatar et al., 2017) and Germany (Ebeling et al., 2021), where it was found that with the exception of pure urban catchments diffuse sources rather than point sources control the C-Q shape in typical European mixed land use settings. Also, we do not consider other loading processes that may create bending at the catchment outlet (e.g., shifts in transport pathways and solute sources, Marinos et al. 2020).

$$L_{in,i} = \underbrace{L_{in.up,i}}_{\text{Upstream Loads}} + \underbrace{L_{in.ls,i}}_{\text{Direct Land to stream Loading}} = \sum_j W_{ji} L_j + c * (Q_{t.sp} * a_i)^{b+1} \quad (3)$$

The modelled in-stream  $\text{NO}_3^-$  uptake follows first order removal kinetics (Alexander et al., 2000; Boyer et al., 2006; Ensign and Doyle, 2006), such that the outgoing load from grid cell  $i$ ,  $L_i$  [ $\text{mg s}^{-1}$ ] is a fraction of the incoming load  $L_{in,i}$  (Eq. (4)) and the absolute removed load  $L_{r,i}$  [ $\text{mg s}^{-1}$ ] can be described as (Eq. (5)). Here,  $L_{r,i}$  is influenced by separate hydrological ( $\frac{P_i * l_i}{Q_i}$ ) and biological ( $v_f$ ) components (similar to Bertuzzo et al., 2017).

$$L_i = L_{in,i} * e^{-\frac{v_f * P_i * l_i}{Q_i}} \quad (4)$$

$$L_{r,i} = L_{in,i} - L_i = L_{in,i} * (1 - e^{-\frac{v_f * P_i * l_i}{Q_i}}) \quad (5)$$

where  $P_i$  is the cross section wetted perimeter calculated from the Manning equation (using the bed slope  $S_i$  and assuming a fixed roughness coefficient = 0.03 [ $\text{m}^{-1}$ ]) in open channels (Eq. (A2)). The uptake velocity parameter  $v_f$  [ $\text{m day}^{-1}$ ] refers to the vertical movement of  $\text{NO}_3^-$  molecules from the water column towards the biofilm at the pelagic-benthic interfaces and the sediments where the in-stream processing chiefly occurs with  $v_f = k_i d_i$  and  $k_i$  the first order removal constant (Ensign and Doyle, 2006; Wollheim et al., 2006; Marcé et al., 2018). The parameter  $v_f$  accounts for the processes altering the rate and form of downstream  $\text{NO}_3^-$  delivery (Doyle, 2005) (therefore it is not limited to denitrification only). We assume that  $v_f$  is independent of the in-stream  $\text{NO}_3^-$  concentration  $C_{mean}$  (Pennino et al., 2014; O'Brien et al., 2007) such that the areal uptake rate  $U = v_f * C_{mean}$  [ $\text{mg m}^{-2} \text{day}^{-1}$ ] is tightly linked with  $C_{mean}$  in a first order relationship. Others (e.g., Hensley et al., 2014; Mulholland et al., 2008; O'Brien et al., 2007) contrarily found explicit scaling relationships where  $v_f$  decreases non-linearly for increasing  $C_{mean}$  ( $10^{-4} - 10^1 \text{ mg L}^{-1}$ ) when considering distinct catchments. However, in Germany, the  $\text{NO}_3^-$  concentration range across a range of catchments is small ( $10^{-1} - 10^1 \text{ mg L}^{-1}$  according to Ebeling et al., 2021) and rivers generally have minor longitudinal concentration variability (Hensley et al., 2014; Ensign and Doyle, 2006) which suggest independent definitions of  $v_f$  and  $C_{mean}$ .

The Damköhler number  $Da$  [-] is calculated as the ratio between transport ( $\tau_T$ ) and reaction ( $\tau_R$ ) timescales and is often used to characterize the relative importance of hydrological and biogeochemical processes in hydrological connected systems (Oldham et al., 2013; Kumar et al., 2020):

$$Da = \frac{\tau_T}{\tau_R} = \frac{TT}{k^{-1}} \quad (6)$$

where,  $\tau_T$  represents as the effective travel time,  $TT$  [days] or the exposure time scale under advective conditions. We estimated the catchment wide  $TT$  as the spatiotemporal median of the sum of all downstream  $T_i$  (Eq. (2.4)) for a grid cell in the network ( $\sum_i^{out} T_i$ ) (similar to Bergstrom et al., 2016). Whereas  $\tau_R$  represents the reactive time scale of biological processes. It is approximated as  $k^{-1}$  [days<sup>-1</sup>] with the effective catchment wide  $k$  estimated as the spatiotemporal median of the grid-scale first order reaction constant  $k_i = d_i/v_f$ .

### 2.3 Exploring $Curv_{max}$ with Monte Carlo Simulations

Monte Carlo simulations are performed to explore how  $Curv_{max}$  evolves from a range of model input parameter combinations in a variety of catchments (Sect 2.3.1 below). These simulations utilize the same ensemble of 11107 unique parameter combinations in each of the individual study catchments with distinct observed discharge time series to account for the differences one parameter combination may have in each of the catchments. The unique parameter combinations are generated by Latin Hypercube sampling from uniform parameter ranges that are set according to literature values (Table 1). Some physical constraints were also imposed such that the channel geometry parameters  $a_w$  and  $a_d$  must obey continuity principles ( $a_w + a_d < 1$  and  $a_w > a_d$ , following Leopold and Maddock, 1953). Similar to Bertuzzo et al. (2017) the chosen parameter combination is kept constant in time and uniform in space for simplicity during one model run. The simulated variables are i)  $Curv_{max}$  [-], deduced from simulated log(C)-log(Q) relationships when minimum 80 % of the C data is above the ‘detection limit’ of 0.002 mg L<sup>-1</sup> NO<sub>3</sub><sup>-</sup>; ii) the network wide percentage load removed  $L_{r,perc}$  [%] which is calculated as the median of the ratio between the daily absolute removed load and the daily absolute incoming load in the river network; iii) the median network travel time,  $TT$  [days]; (iv) the Damköhler number  $Da$  [-]; (v) the slope of the linear regression fit of the log(C)-log(Q) relationship at the catchment outlet,  $b_{out}$  [-]; (vi) the median concentration at the catchment outlet,  $C_{out}$  [mg L<sup>-1</sup>] and the median water velocity,  $v$  [m s<sup>-1</sup>]. While all outputs can be spatially and temporally explicit on a daily time step,  $Curv_{max}$  is examined at the catchment outlet, integrating both spatial and temporal aspects. The Monte Carlo results are subsequently subjected to a global sensitivity analysis with the PAWN method (Pianosi and Wagener; 2015) to elucidate influential model parameters. Furthermore a correlation analysis is conducted to explore how these influential parameters impact simulated  $Curv_{max}$ . Finally, a Classification and Regression Tree algorithm (CART, Breiman et al., 1984) allowed us to visualize parameter interactions as detailed in Sect. 2.3.2 below.

**Table 1: Network model parameter ranges for the Monte Carlo simulations.**



Parameter	Unit	Description	Range	References
$v_f$	[m day <sup>-1</sup> ]	Uptake velocity	10 <sup>-4</sup> ; 0.25	Marce et al, 2018 <sup>a</sup>
$b$	[-]	Slope b lin. regress. log(C)-log(Q)	-1.5; 1.5	Musolff et al., 2017, Ebeling, 2020b
$C_{mean}$	[mg L <sup>-1</sup> ]	Land to stream concentration	10 <sup>-4</sup> ; 20	Ebeling, 2020b
$K_w$	[L <sup>1-3*a<sub>w</sub></sup> . T <sup>-a<sub>w</sub></sup> ]	Coefficient width-Q function	2.6; 20.2	Andreadis et al., 2013
$a_w$	[-]	Exponent width-Q function	0.01; 0.54	Andreadis et al., 2013; Dingman, 2007
$K_d$	[L <sup>1-3*a<sub>d</sub></sup> . T <sup>-a<sub>d</sub></sup> ]	Coefficient depth-Q function	0.12; 0.63	Andreadis et al., 2013
$a_d$	[-]	Exponent depth-Q function	0.28; 0.667	Andreadis et al., 2013; Dingman, 2007

250 <sup>a</sup>For  $v_f$ , the selected range is an order of magnitude smaller than the one proposed by Marce et al., 2018 as we focus the analysis on the lower  $v_f$  where most of the bending happens (Sect. 3.3).

### 2.3.1 Catchment selection

The river networks of 13 mesoscale catchments across Germany (areas between 21 and 1450 km<sup>2</sup>, Ebeling, 2020a; Table 2) are extracted together with the corresponding daily discharge data at the outlet (uninterrupted for ~10 years between 1995 and 255 2010 (Musolff, 2020)) as inputs for the exploratory river network model. The selected catchments include three nested sub-catchments for the Selke as well as the Holtemme river system, both part of the Bode, a well-studied river system near the Harz Mountains in central Germany (Fig. 1; Ehrhardt et al., 2019; Rode et al., 2016; Winter et al., 2020; Mueller et al., 2018). All catchments have distinct geophysical settings as stream order, median discharge and catchment shape (quantified with the Horton form factor; Horton, 1945; Table 2) which is needed to obtain a realistic range of simulated  $Curv_{max}$  using the 260 explorative network model in the Monte Carlo mode. The selected catchments were delineated in ArcMap (ESRI, 2011) from a 100 m x 100 m DEM (EEA, 2013; Ebeling et al., 2021). A flow direction, flow accumulation and valley slope grid in the same resolution were established. The channel threshold drainage area for the network delineation was set to 150 grid cells (1.5 km<sup>2</sup>), which agreed well with the observed river network, resulting in a tree shaped river network with N grid cells or nodes.

265

**Table 2: Catchment properties summary: Catchment Area, median Elevation, Slope and Topographical Wetness Index (TWI), maximum Strahler Stream Order, Horton form factor, Drainage Density, median discharge at the basin mouth over time (Q) with the corresponding runoff (area specific discharge) between brackets and the coefficient of variation of the discharge in time (CV Q). The latter variable CV Q integrates the frequency of runoff events and the differences in recession constant (so the catchments 270 “flashiness” in response to rainfall) (Botter et al., 2013).**

ID	River	Area	Med. elevation	Med. slope	Med. TWI	Stream order	Network length	Horton form factor	Drainage density	Med. Q	CV Q
		[km <sup>2</sup> ]	[m]	[°]	[-]	[-]	[km]	[-]	[km km <sup>-2</sup> ]	[m <sup>3</sup> s <sup>-1</sup> ] (mm day <sup>-1</sup> )	[-]
1	Dahme	20.9	105	1.50	10.08	2	11	0.67	0.52	0.02 (0.07)	1.13
2	Kraichbach	422.5	164	2.84	9.45	4	228	0.23	0.54	0.85 (0.17)	0.47
3	Wertach	658.1	833	4.30	9.17	4	391	0.14	0.59	10.60 (1.39)	0.96
4	Ammer	713.7	858	8.34	8.80	4	416	0.29	0.58	14.98 (1.81)	0.84

5	<i>Modau</i>	88.6	272	5.61	8.47	3	47	0.42	0.53	0.52 (0.51)	0.80
6	<i>Leine</i>	993.2	276	4.40	8.95	4	525	0.45	0.53	6.22 (0.54)	0.85
7	<i>Speyerbach</i>	142.0	187	3.58	9.84	3	104	0.17	0.73	0.66 (0.40)	0.64
8	<i>Stör</i>	1452.2	25	0.90	10.63	5	905	0.46	0.62	14.10 (0.84)	0.76
9	<i>Holtemme</i>	272.5	258	3.58	9.49	4	145	0.17	0.53	1.04 (0.33)	1.01
10	<i>Selke Silberhütte</i>	94.5	456	4.02	8.72	3	49	0.27	0.51	0.56 (0.51)	1.34
11	<i>Selke Meisdorf</i>	282.1	342	3.94	9.03	3	160	0.35	0.57	0.70 (0.21)	1.34
12	<i>Selke Hausneindorf</i>	460.1	263	2.90	9.60	4	256	0.37	0.56	0.65 (0.12)	1.50
13	<i>Schleuse</i>	263.2	597	9.12	7.92	4	139	0.79	0.53	2.88 (0.95)	1.07

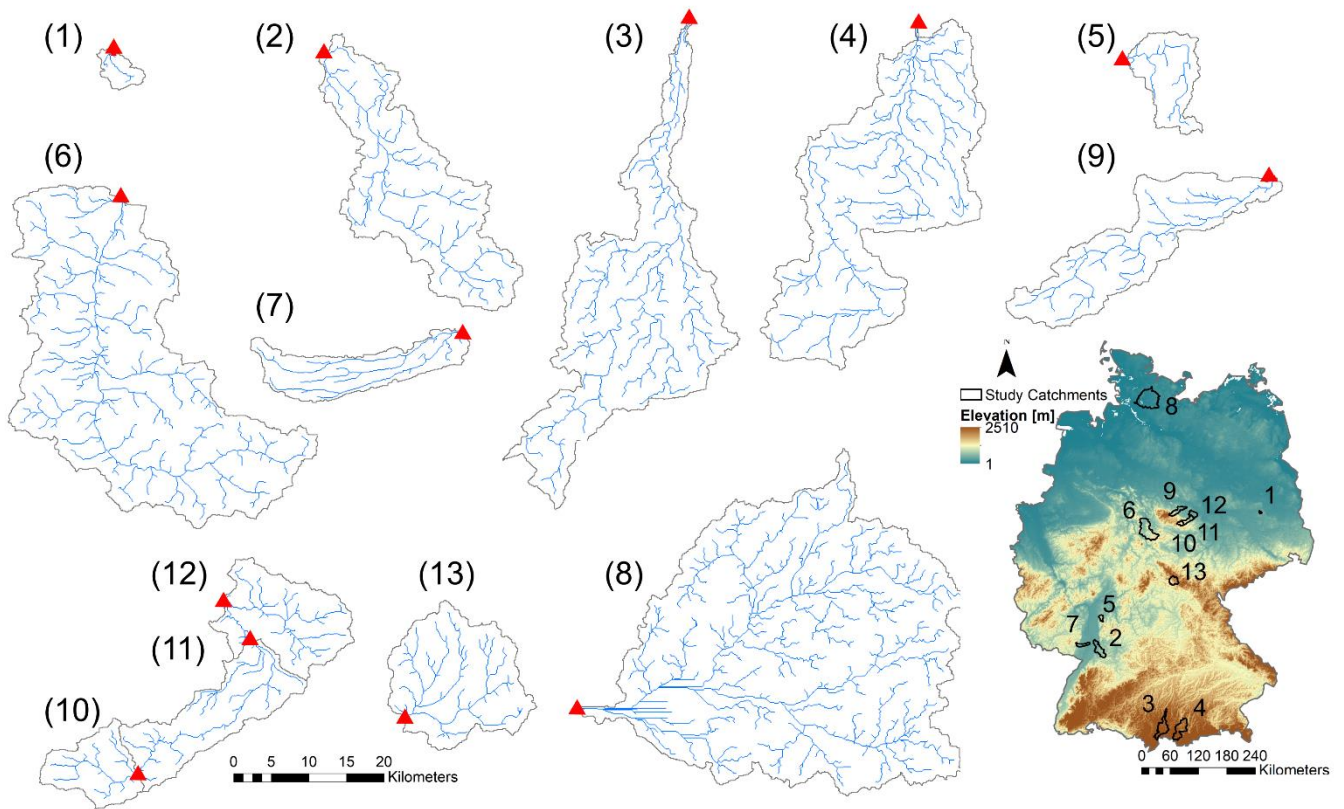


**Figure 1: Germany DEM with the location and outline (shape) of selected catchments, along with their drainage networks (in blue) and outlet location (red triangle). See Table 2 for catchment ID's and properties.**

### 275 2.3.2 Model evaluation

To verify the network model's ability to reproduce realistic concentration time series and  $Curv_{max}$ , the observed monthly nitrate concentrations and the simulated time series were compared in one of the 13 selected catchments, the Selke catchment (at Meisdorf gauging station; 282 km<sup>2</sup>, Table 2; Winter et al., 2020) where extensive field campaigns and modelling studies have

been conducted related to in-stream processes (Rode et al., 2016; Dupas et al., 2017; Yang et al., 2019; Yang et al., 2018).  
 280 Note that such a model validation was performed only in the Selke Meisdorf catchment as the model aim is to explore how  
 certain input parameter combinations may result in log(C)-log(Q) bending at the catchment outlet, rather than to reproduce  
 catchment specific concentrations by performing parameter calibration. This explorative approach is comparable to Bertuzzo  
 et al., (2017) and Helton et al., (2018) who applied a similar model in synthetic river networks but did not validate the model  
 structure in a realistic setting. The Meisdorf catchment is a relatively homogeneous upstream part of the Selke, consisting of  
 285 forest and cropland and is characterized by constant export regimes (Winter et al., 2020). For an input parameter combination  
 set to reasonable values for this catchment (Table C1; Rode et al., 2016), the land to stream  $\text{NO}_3^-$  inputs averaged  $1.2 \text{ kg N day}^{-1} \text{ km}^{-2}$   
 which is similar to the  $1.9 \text{ kg N day}^{-1} \text{ km}^{-2}$  reported by Winter et al. (2020) for the Selke River (Meisdorf); and it  
 is well within the general  $0.001$  to  $100 \text{ kg N day}^{-1} \text{ km}^{-2}$  range established by Mulholland et al. (2008). The simulated flow  
 velocity had a spatiotemporal median value of  $0.47 \text{ m s}^{-1}$ , which is also comparable with measured flow velocities (Risse-Buhl  
 290 et al., 2017). Additionally, the Selke catchment was used to gain an insight into how the interplay of transport and uptake  
 processes at every network grid cell can result in a curved C-Q pattern at the catchment outlet for one parameter combination,  
 while in the other catchments the network model outputs were only considered at the catchment outlet for the entire range of  
 input parameter combinations in the Monte Carlo approach. Finally, the simulated range of  $Curv_{max}$ , obtained from applying  
 the network model in the 13 different catchments with  $>10000$  input parameters, was compared to a range of observed  $Curv_{max}$   
 295 computed from the C-Q relationships of 444 French catchments (Dupas et al., 2019; Sect. 2.1). Other Monte Carlo simulation  
 outputs, such as ranges of  $L_{r,perc}$  and  $Da$  were compared to literature values for validation purposes.

### 2.3.3 PAWN sensitivity analysis and correlation analysis

We performed a global sensitivity analysis (GSA) using the moment independent PAWN method (Pianosi and Wagener  
 300 (2015)). The method allowed for estimating the effect of the parameter inputs on the entire model output distribution and can  
 be applied to rank the inputs and identify the uninfluential ones. The resulting PAWN sensitivity indices were estimated from  
 generic input-output samples created with the numerical approximation strategy proposed by Pianosi and Wagener (2018).  
 With this strategy, the range of variation of each input  $x_i$  is partitioned into a number  $n_i$  of equally probable ‘conditioning’  
 intervals ( $I_{i,k}$ ,  $k = 1, \dots, n_i$ ), i.e. each interval contains the same number of data points. Given a scalar model output  $y$  (here  
 305  $Curv_{max}$ ), the PAWN method compares the output conditional Cumulative Distribution Function (CDF) ( $F_y(y)$ ), computed by  
 concurrently varying all the inputs, and the  $n_i$  conditional CDFs for that input ( $F_{y|x_i}(y|x_i \in I_{i,k})$ ). Each conditional CDF is  
 obtained by varying all inputs within their entire range except for  $x_i$ , whose values are contained within one of the  $n_i$   
 conditioning intervals. The Kolmogorov-Smirnov statistic (KS) is then calculated as the maximum vertical distance between  
 the conditional and unconditional CDFs, while the PAWN sensitivity index ( $S_i$ ) for input  $x_i$  aggregates the results over all  
 310 conditional CDFs through a summary statistic as presented in Eq. (7):

$$S_i = \text{stat}_{k=1 \dots n_i} KS(I_{i,k}) \quad (7)$$

where  $KS(I_{i,k}) = \max_y |F_y(y) - F_{y|x_i}(y|x_i \in I_{k,i})|$

In this study, we applied Eq. (7) using  $n_i = 10$  conditioning intervals for each input parameter and used the maximum KS value,  $KS_{max}$  (ranging from 0 to 1), as a summary statistic, which is appropriate for screening non-influential input parameters.

315 For a given parameter, the highest value of  $KS_{max}$  of 1 would indicate a direct dependence of the model output (in this case  $Curv_{max}$ ) on that parameter, while a value of  $KS_{max}$  of 0 would mean that the parameter is completely non-influential. We estimated confidence intervals of the sensitivity indices using 15000 bootstrap resamples and checked the robustness of the results. The PAWN analysis was carried out using the Python version of the SAFE toolbox for global sensitivity analysis (Pianosi et al., 2015).

320

To explore the direction of change in the C-Q bending at the catchment outlet resulting from variations in the model parameters and the catchment in-stream uptake, a Spearman rank correlation analysis was performed including all the simulated catchment responses and parameter combinations. These correlations were visualized in a correlation matrix using the ‘corrplot’ package in R (Wei and Simko, 2020).

325

### 2.3.4 Identify parameter and model output interactions with classification tree

Finally, we aim to determine if, within this modelling framework, C-Q bending at the catchment outlet (specifically  $Curv_{max}$ ) informs about the network wide in-stream uptake. Thereto, a recursive modelling approach is proposed, using the Classification and Regression Trees algorithm (CART, Breiman et al., 1984) which allows for the identification of non-linear synergistic interactions among model parameters and output variables. This non-parametric method segregates classes for a response variable by progressively splitting selected predictor variables in a binary way. The resulting decision tree is intuitive to interpret and can facilitate the fast characterization of river networks. The response variables include the effective catchment wide removal efficiency  $L_r$ , the Damköhler number  $Da$  and the uptake velocity  $v_f$ , while the predictors are  $Curv_{max}$ , the median network velocity  $v$  and all of the model input parameters except for  $v_f$  (Table 1). For each response variable, three classes are defined representing low, intermediate and high ranges found in the literature (Table 3) that each contain 5 % of the simulation outputs (obtained by distributing the non-missing model simulations over 20 percentiles). The overall CART accuracy for each response variable is assessed by attributing 80 % of the simulation outputs in the low, intermediate and high classes to a training sample and assigning the remaining 20 % to a test sample. The training sample is then used to construct the classification tree while the test sample is needed to assess the prediction accuracy and calculating the performance statistics for each class. The CART analysis was performed using the ‘caret’ package in R with the Gini impurity measure as splitting criterion (Kuhn, 2020).

340

**Table 3: Classes containing low, medium and high values for response variables  $v_f$  (uptake velocity),  $L_{r,perc}$  (percentage load removed) and  $Da$  (Damköhler number) are used for the CART training and testing samples. Similar classes are obtained for model**

345 output  $Curv_{max}$ . These classes stem from distributing the non-missing simulation data over 20 percentiles and selecting the percentiles corresponding to low, medium and high literature values with the respective percentile number (1-20) indicated in brackets. This was done to ensure that for one variable, each class contains the same amount of simulation data points. The training sample for constructing the CART model was then allocated 80% of this data and the test sample 20 %.

Variable	Units	Low	Medium	High	References
$v_f$	[ $m\ day^{-1}$ ]	$10^{-4}$ -0.01 (1)	0.10-0.11 (10)	0.23-0.24 (20)	Birgand et al., 2007, Marce and Armengol, 2009
$L_{r,perc}$	[%]	3.8-5.2 (7)	28.7-35.1 (15)	63.0-75.3 (19)	Birgand et al., 2007
$Da$	[-]	0.17-0.25 (3)	0.88-1.02 (10)	3.25-4.19 (18)	Oldham et al., 2013
$Curv_{max}$	[-]	-0.70;-0.51 (3)	-0.25;-0.22 (9)	-0.03;-0.01 (18)	Dupas et al., 2019

### 350 3 Results and Discussion

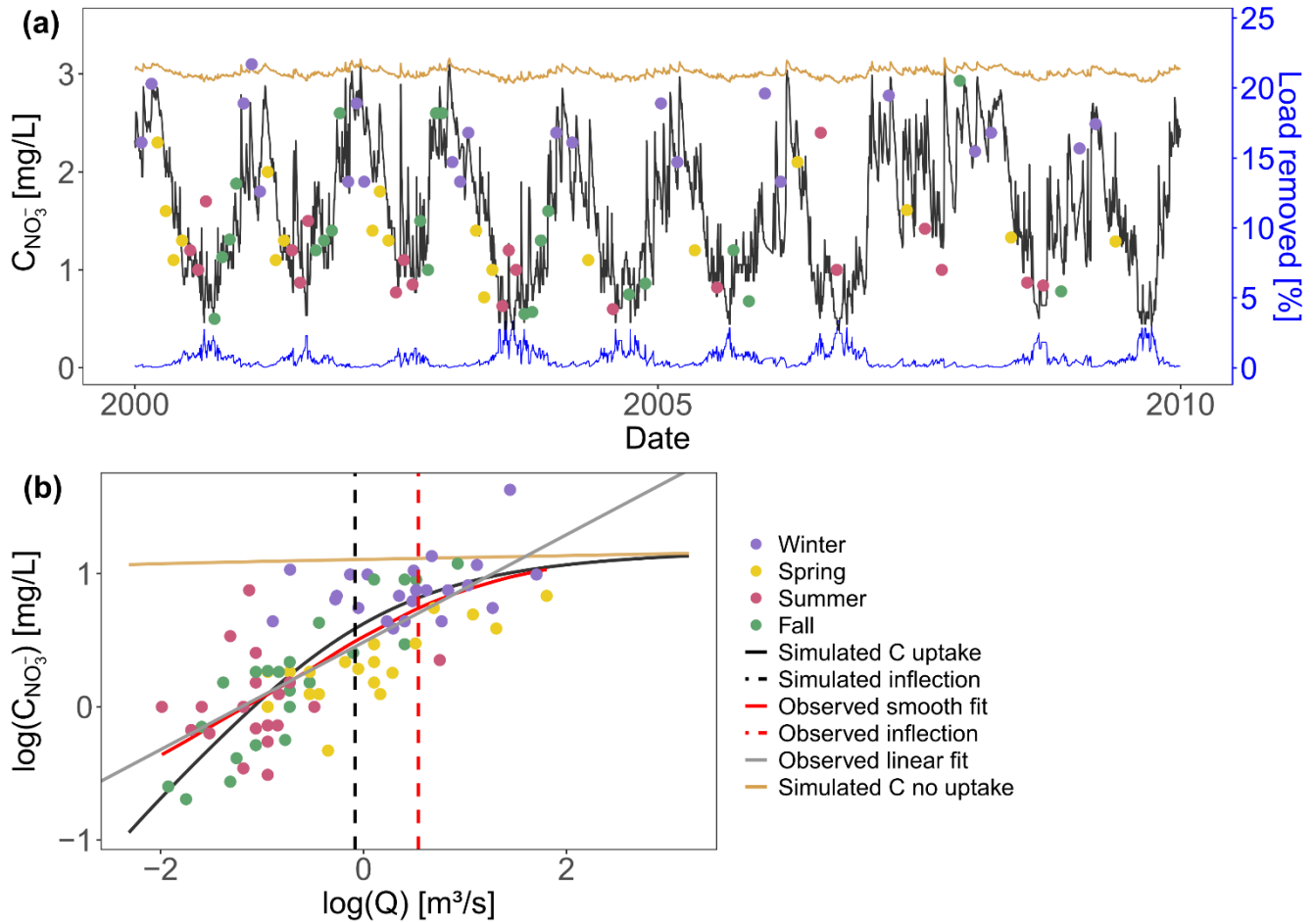
#### 3.1 Empirical $Curv_{max}$

The estimated  $Curv_{max}$  for the French observed  $NO_3^-$  log(C)-log(Q) data (Dupas et al., 2019) ranges between -5.25 and 3.88 (median is -0.23, Fig. B4) and 77 % of the stations are characterized by  $Curv_{max} \leq 0$  or a linear or concave shape (similar to Moatar et al. 2017). The time series subsamples for each station generally had a small  $Curv_{max}$  variability (Interquartile Range, 355 IQR for a given station below 1) for 93 % of the stations with some exceptions demonstrating a larger IQR up to 8. This indicates  $Curv_{max}$  quantification for most low frequency C-Q time series is robust. The Spearman rank correlation ( $\rho = 0.53$ , p-value  $< 2.2e-16$ ) between the absolute observed  $Curv_{max}$  and IQR for each station is significant and positive, implying that C-Q relationships with a higher absolute  $Curv_{max}$  have a higher uncertainty when quantifying the C-Q bending. However,  $Curv_{max}$  variability (IQR) in the subsamples for each station has no significant correlation with the number of data points 360 available for one station. This implies that  $Curv_{max}$  tends to be temporally robust when the C-Q data obeys the four criteria in Sect. 2.1 so that the length of the low frequency time series length does not impact the estimated  $Curv_{max}$ . Overall, the proposed  $Curv_{max}$  metric is suitable to quantify bending in multiannual, temporally stable log(C)-log(Q) relationships.

#### 3.2 Model evaluation in the Selke River (Meisdorf)

365 To evaluate the network model performance in a realistic setting, we implemented the model with a fixed parameter combination (Table C1) in the Selke catchment and aimed to capture C-Q dynamics at the basin outlet. The simulated  $NO_3^-$  concentration time series (simulated C with uptake) for the Meisdorf station in Fig. 2a shows a seasonal pattern that follows the observation concentration data reasonably well (Nash-Sutcliffe Efficiency; NSE = 0.50, percent bias; pbias = -0.4 %). This seasonality is also reflected in simulated daily percentage of load removed (the ratio between the daily total removed load and 370 the daily total incoming load in the river network); and ranges from almost 0 % to 3.4 % in this case, with the median  $L_{r,perc}$  value equal to 0.41 %. The highest removal efficiencies are simulated in fall and summer and coincide with low simulated  $NO_3^-$  concentrations at the catchment outlet. The conservative  $NO_3^-$  concentration (simulated C no uptake) is stable around 3 mg L<sup>-1</sup>. The observed nitrate concentrations generally show an enrichment export pattern in the log(C)-log(Q) space ( $b_{out} =$

0.40,  $R^2 = 0.56$ ) and a  $Curv_{max}$  of -0.35 which agrees well with the simulated  $Curv_{max}$  of -0.28 (Fig. 2b) and deviates significantly from the conservative scenario of simulated C without uptake ( $b=0.014$ ; Table C1). The observed low nitrate concentrations coincide with low discharges in fall and summer, while high concentrations occur mainly in winter when discharges are higher.



380 **Figure 2:** (a) Simulated and observed  $NO_3^-$  concentrations at the Selke Meisdorf gauging station for a 10 year simulation period (2000-2010; NSE=0.50). One data point ( $C \sim 5 \text{ mg L}^{-1}$ ) is not shown here. The simulated median percentage of load removed in the stream network (blue line) is given during the same time period as well as the simulated C with no uptake ( $v_f=0$ ). (b) The observed  $NO_3^-$  concentrations and Q are log transformed and plotted together with the simulated C-Q data for 2000-2010. A smoothed spline is fitted to the observed and simulated C-Q data (described as observed smooth fit and simulated C respectively in the legend); and  $Curv_{max}$  of -0.35 and -0.28 are calculated at the respective discharges of  $1.72 \text{ m}^3 \text{ s}^{-1}$  and  $0.92 \text{ m}^3 \text{ s}^{-1}$ , indicating the smoothed spline inflection points.

385

Within the Selke Meisdorf river network the simulated  $Curv_{max}$  is largely contained within -1.12 to -0.29 (10<sup>th</sup> and 90<sup>th</sup> quantiles respectively) for the given parameter combination (Table C1, Fig. 3). Low  $Curv_{max}$  ( $< -1.12$ ) is found exclusively at grid cells with a low total drainage area ( $A_i < 9 \text{ km}^2$ ) and  $Curv_{max}$  stabilizes at higher values with increasing drainage areas (inset Fig. 3, Fig. S3 in Supporting Information). The incoming ( $L_{in.ls}$  and  $L_{in.up}$ ; Eq. (3)), removed ( $L_r$ ; Eq. (5)) and outgoing absolute load ( $L_i$ ; Eq. (4) with  $L = CQ$ ) as function of  $Q$  in the log-log space are shown in Fig. 3 for three selected grid cells on the main river stem with low (C), intermediate (B) and high (A) drainage areas. The corresponding log(C)-log(Q) relationship for the outgoing load ( $L_i$ ) at the outlet (A) is presented in Fig. 2b for simulated and observed values. Note that  $Curv_{max}$  is calculated from log(C)-log(Q) relationships rather than log(L)-log(Q). The loads in grid cell A, B and C generally increase with discharge while the load removal efficiency decreases with discharge. The highest removal efficiencies are found in the headwater grid cell C (39 % for low discharge), followed by mid-stream grid cell B (3 % for low discharge) and the outlet A (0.5 % for low discharge). The total absolute load removed ( $L_r$ , sum per year per grid cell) is largest for first order grid cells (average 24.1 kg N year<sup>-1</sup>) that represent 55 % of the river network, followed by second and third order grid cells (averaging both around 20 kg N year<sup>-1</sup>) that represent 20 and 25 % of the network (inset Fig. 3). Finally, the total yearly incoming load ( $L_{in.ls} + L_{in.up}$ , sum per year per grid cell) increases with stream order from 1329 kg N year<sup>-1</sup> on average in a first order grid cell to 5128 and 42124 kg N year<sup>-1</sup> in second order and third order river cells.

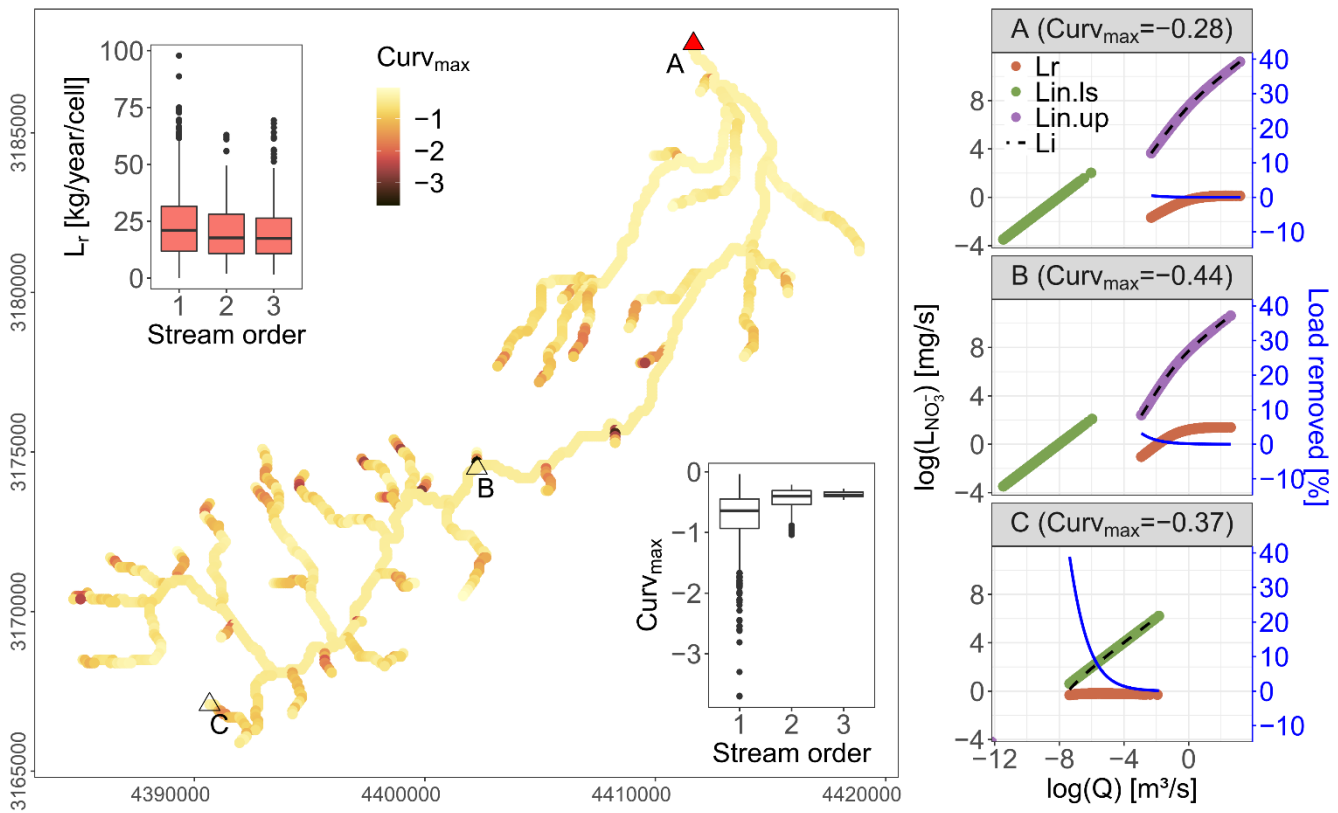


Figure 3: Spatial distribution of simulated  $Curv_{max}$  in the Selke river network (Meisdorf) for a selected parameter set (see Table C1). Three representative grid cells covering low (A), intermediate (B) and high (C) total drainage areas show the incoming land to stream load as  $L_{in.ls}$  (Eq. (3)), the incoming load from upstream as  $L_{in.up}$  (Eq. (3)), the absolute removed load as  $L_r$  (Eq. (5)) and the outgoing load as  $L_i$  (Eq. (4)) in the  $\log(L)$ - $\log(Q)$  space. The load removed as a percentage of the incoming load is presented on the secondary axis. Note that the corresponding  $Curv_{max}$  for these grid cells are calculated from the  $\log(C)$ - $\log(Q)$  relationships rather than  $\log(L)$ - $\log(Q)$ . The insets show the distribution of  $Curv_{max}$  and  $L_r$  for each of grid cells within a certain stream order. In Fig. 2a the observed and simulated concentrations are compared at point A.

410

With uniform, constant parameters the network model does not account for a spatiotemporal parameter variability. Nevertheless, it successfully (see NSE and pbias) reproduces the seasonality of the observed concentrations over the 2000-2010 period for the Selke Meisdorf catchment (Fig. 2a). For comparison, Yang et al. (2018) found a similar performance (NSE = 0.47, pbias = -3.35 %) when applying a fully distributed model with 16 calibrated parameters in this catchment between 1997 and 2009. The uptake velocity  $v_f$  for our simulation was set to  $0.098 \text{ m day}^{-1}$  to closely match the observed (assimilatory) uptake range of  $0.009$  to  $0.103 \text{ m day}^{-1}$  for the Selke Meisdorf river network (Rode et al., 2016), the median annual percentage load removed equals 4.7 % which is within a comparable range reported in prior studies (Rode et al., (2016) and Yang et al., (2018) found annual means of 4.8 and 7.6 % respectively). Note that the annual percentage load removed accounts for load taken up throughout the entire river network, which may be higher in the headwaters (15 tons) than in downstream locations (7 and 5 tons for second and third order stream sections; inset Fig. 3). Yang et al. (2018) reported very high uptake efficiencies (up to 75 %) for summer seasons that were caused by low  $\text{NO}_3^-$  concentrations ( $0.21 \text{ mg N L}^{-1}$ ) and load ( $L = CQ$ ), which are not represented in our model simulation (the lowest simulated  $\text{NO}_3^-$  concentration equaled  $0.4 \text{ mg N L}^{-1}$ ). Additionally, due to the parsimonious structure of the proposed model, we did not account for the temporally changing effects of environmental factors like temperature and light availability that might (seasonally) influence uptake efficiencies in the river network (Kadlec and Reddy, 2001). Nevertheless, these reported high low flow uptake efficiencies in summer are not a main contributor to the annual percentage load removed that is dominated by high flows, generally recorded during winter. Thus for the Monte Carlo simulations (Sect. 3.2 below) we calculated  $L_{r.perc}$  as the median of the daily percentage load removed rather than the total removal efficiency for the entire simulated time period to better represent an effective long term network wide removal capacity.

430

The interplay of incoming, removed and outgoing load at each network grid cell shapes the  $\log(L)$  and  $\log(C)$ - $\log(Q)$  relationships and consequently  $Curv_{max}$  at the catchment outlet (Fig. 3). Land to stream loading ( $L_{in.ls}$ ) that varies linearly with direct incoming discharge at a given grid cell in the  $\log$  space (Eq. (3) with  $L = CQ$ ;  $Curv_{max} = 0$ ) can lead to a bent outgoing  $\log(C)$ - $\log(Q)$  relationship where concentration or load ( $L_i$ ) varies non-linearly with discharge ( $Curv_{max} \neq 0$ ). The onset of a bent  $\log(C)$ - $\log(Q)$  pattern ( $Curv_{max} = -0.37$ ) is illustrated in the headwater grid cell C in Fig. 3 where  $L_{in.ls}$  is the only incoming load (upstream incoming load,  $L_{in.up}$  equals 0 in this case). The absolute removed load in a grid cell is higher under increasing



Q while the percentage load removed is lower, which explains observed C-Q patterns with higher  $\log(C)$ - $\log(Q)$  slopes for low flows than for high flows (Moatar et al., 2017; Wollheim et al., 2008; Doyle, 2005; Wollheim et al., 2017; Basu et al., 2011). This decreased  $\text{NO}_3^-$  load removal efficiency in the downstream direction (spatial scale) or during events (temporal scale) can arise because stream morphology characteristics such as depth and water velocity, that correlate with varying discharge, constitute higher surface-to-volume ratios at low flows (generally in the headwaters) than at higher flows (at the outlet) (Peterson et al 2001; Hensley et al 2014). The uptake and land to stream loading at the downstream grid cells (B and A in Fig. 3) have a decreasing local impact on the outgoing load due to the large upstream load contributions that increase in the downstream direction (see explicit scaling relationship for input flux in Bertuzzo et al., 2017). This is also explained by Wollheim et al. (2018) who suggests that the river network saturates as supply exceeds biological ‘demand’, causing the  $\log(C)$ - $\log(Q)$  relationship to approach the slope of the loading function (presented as the simulated C without uptake in Fig. 2b). Dupas et al. (2017) on the other hand shows how  $\text{NO}_3^-$  uptake effects are decreasingly visible in C-Q observations downstream and concentrations largely matched those estimated by a conservative mixing model. The saturation effect with the accumulation of large load is reflected in the  $Curv_{max}$  converging to a constant value when moving from upstream to downstream or from a lower order to a higher order river reach (Fig. 3; Fig. S3). This also corroborates the recent findings of Abbott et al. (2018) who found that the temporal variability (here reflected in the C-Q relationship) of nutrients is preserved moving downstream in a river network. Overall the Selke example shows that the network model can realistically reproduce the bending of observed  $\text{NO}_3^-$  C-Q relationships that evolve from the decreasing removal efficiency at higher discharges.

### 3.2 Monte Carlo simulation results

The overview of the model outputs for each of the 13 study catchments in Table 4 shows that catchments 1, 5 and 11 display the lowest 10<sup>th</sup> quantile  $Curv_{max}$  values of -1.61, -1.40 and -1.24 (more bending) while the catchments 4 and 6 registered higher (less bending) and less variable  $Curv_{max}$  (10<sup>th</sup> quantiles at -0.31 and -0.35) (Fig. B5). Catchments 3, 4 and 8 are characterized by high runoff and Q (Table 2) at the catchment outlet and demonstrate low percentages of load removed,  $L_{r.perc}$  (90<sup>th</sup> quantile at 29.8, 32.1 and 19.3 % respectively). The highest  $L_{r.perc}$  are found in catchments 1 and 10 (98.4 and 95.1 % for the respective 90<sup>th</sup> quantiles). The regression slope of the  $\log(C)$ - $\log(Q)$  relationship at the basin outlet,  $b_{out}$ , is positively skewed for all the catchments (most positive slopes found in catchment 5) while the slope  $b$  of the land-to stream loading function had no positive or negative preference (Table 1, Eq. (3)). The distribution of the concentrations at the catchment outlet,  $C_{out}$ , are generally similar across all catchments (10<sup>th</sup> and 90<sup>th</sup> percentiles within 0 to 6.2 mg L<sup>-1</sup>) and are significantly less variable than the land-to-stream incoming concentration (parameter  $C_{mean}$ ) that varied from 10<sup>-4</sup> to 20 mg L<sup>-1</sup> across all the simulations (Table 1). The highest  $C_{out}$  are found in the largest catchment 8. The median water velocity  $v$  (Eq. (2.3)) is between 0.01 and 0.5 m s<sup>-1</sup> for the 10<sup>th</sup> and 90<sup>th</sup> quantiles of all the study catchments and the largest  $v$  is simulated for catchments 3 and 4 that also have the highest discharge. The median river network travel time,  $TT$ , for all simulations and catchments ranges from 0.1 to 4 days between their respective 10<sup>th</sup> and 90<sup>th</sup> quantiles and remarkably have no clear relationship with catchment properties as the

470 total river network length (Table 2). Finally, the Damköhler number,  $Da$  (Eq. (6)), is variable around 1 with the highest values, indicating reaction driven conditions, found for catchments 2 and 12 (respective ranges from 0.6 to 10.3 and 0.7 to 10.8 for the 10<sup>th</sup> and 90<sup>th</sup> quantiles). The lowest  $Da$  values are found for catchments 4 and 10 (90<sup>th</sup> quantile < 2) implying more transport driven conditions.

475 **Table 4: The 10<sup>th</sup>, 50<sup>th</sup> and 90<sup>th</sup> quantiles of model outputs  $Curv_{max}$ , percentage load removed,  $L_{r.perc}$ , Damköhler number  $Da$ , regression slope of the log(C)-log(Q) relationship at the basin outlet,  $b_{out}$ , the median concentration at the basin outlet,  $C_{out}$ , the median water velocity,  $v$  and median river network travel times,  $TT$ , for each of the 13 German catchments.**

Catch. ID	$Curv_{max}$ [-]			$L_{r.perc}$ [%]			$Da$ [-]			$b_{out}$ [-]			$C_{out}$ [mg L <sup>-1</sup> ]			$v$ [m s <sup>-1</sup> ]			$TT$ [days]		
	10 <sup>th</sup>	50 <sup>th</sup>	90 <sup>th</sup>	10 <sup>th</sup>	50 <sup>th</sup>	90 <sup>th</sup>	10 <sup>th</sup>	50 <sup>th</sup>	90 <sup>th</sup>	10 <sup>th</sup>	50 <sup>th</sup>	90 <sup>th</sup>	10 <sup>th</sup>	50 <sup>th</sup>	90 <sup>th</sup>	10 <sup>th</sup>	50 <sup>th</sup>	90 <sup>th</sup>	10 <sup>th</sup>	50 <sup>th</sup>	90 <sup>th</sup>
1	-1.61	-0.32	-0.01	2.6	61.0	98.4	0.3	1.8	6.4	-0.65	0.81	2.22	<10 <sup>-4</sup>	0.06	4.68	0.01	0.06	0.25	0.1	0.5	1.8
2	-1.04	-0.21	-0.01	0.9	19.4	78.5	0.6	3.5	10.3	-0.42	0.95	2.31	<10 <sup>-4</sup>	0.08	2.36	0.02	0.08	0.29	0.6	1.7	3.9
3	-0.43	-0.21	-0.02	0.2	3.5	29.8	0.2	0.9	2.8	-0.54	0.72	1.96	0.01	0.42	5.27	0.07	0.17	0.48	0.5	1.4	3.3
4	-0.33	-0.18	-0.01	0.2	4.2	32.1	0.1	0.5	1.5	-0.60	0.63	1.85	0.03	0.52	5.56	0.07	0.17	0.50	0.3	0.8	1.9
5	-1.40	-0.20	-0.01	1.3	25.6	85.1	0.1	0.7	2.0	-0.49	0.93	2.43	0.01	0.22	3.76	0.04	0.12	0.38	0.2	0.6	1.5
6	-0.35	-0.12	-0.02	0.5	9.7	54.6	0.3	1.5	4.3	-0.58	0.61	1.84	0.02	0.27	3.75	0.04	0.11	0.36	0.4	1.2	2.7
7	-0.44	-0.17	-0.01	0.8	14.3	72.6	0.2	1.3	3.6	-0.52	0.79	2.09	0.01	0.29	4.4	0.04	0.12	0.38	0.4	1.2	2.8
8	-0.63	-0.26	-0.01	0.1	2.9	19.3	0.2	1.4	4.1	-0.71	0.48	1.70	0.07	0.65	6.24	0.05	0.13	0.39	0.5	1.3	3.0
9	-0.68	-0.24	-0.01	0.8	15.0	70.4	0.3	1.9	5.3	-0.53	0.73	1.99	0.01	0.22	3.43	0.04	0.11	0.35	0.5	1.4	3.1
10	-0.79	-0.25	-0.01	1.9	36.8	95.1	0.1	0.7	1.9	-0.45	0.91	2.33	0.01	0.16	3.88	0.04	0.11	0.36	0.2	0.5	1.2
11	-1.21	-0.19	-0.01	1.6	26.1	85.6	0.5	2.6	7.4	-0.48	0.91	2.35	<10 <sup>-4</sup>	0.13	2.41	0.03	0.09	0.32	0.5	1.5	3.5
12	-0.97	-0.22	-0.01	1.5	29.0	83.2	0.7	3.7	10.8	-0.49	0.79	2.07	<10 <sup>-4</sup>	0.08	2.43	0.02	0.08	0.29	0.5	1.6	4.1
13	-0.46	-0.16	-0.01	1.3	18.3	72.9	0.1	0.5	1.5	-0.72	0.48	1.69	0.05	0.47	4.35	0.05	0.14	0.42	0.2	0.6	1.4

The Monte Carlo output in Table 4 shows reasonable values for the different variables, taking into account that the goal of this  
480 modelling exercise was not to reproduce catchment specific conditions but rather explore how NO<sub>3</sub><sup>-</sup> uptake influences C-Q  
bending for a range of parameter combinations that represent a spectrum of possible catchment conditions. The simulated  
 $Curv_{max}$  for all 13 German study catchments and parameter combinations (80 % of the values between -0.70 and -0.012, Table  
4 and Fig. B5) are comparable with the range of  $Curv_{max}$  from NO<sub>3</sub><sup>-</sup> log(C)-log(Q) relationships in the French catchments (80%  
of the values between -0.41 and -0.067; Fig. B4) (Dupas et al., 2019). Simulated  $Curv_{max}$  is always smaller than or equal to  
485 zero as explained in Sect. 2.2.2. For the model output  $L_{r.perc}$ , a wide range of uptake efficiencies were captured from almost  
0 to near to 100 % for some simulations and a median value of 14.4 % across simulations. This simulated range exceeds the  
proposed range by Birgand et al. (2007) of 10 to 70% of N removal for agricultural drainage networks at annual time scales.  
High removal percentages (median over the simulated time period of daily percentage load removed in the network exceeding  
95 %) are registered for 3.4 % of all simulations while very limited load removal ( $L_{r.perc} < 5$  %) occurred for 32.1 % of all the

490 simulations. Other simulation outputs such as the effective velocity  $v$  surprisingly rendered similar distributions across the catchments (Table 4) given that the median  $Q$  varied for almost three orders of magnitude at the basin outlet (Table 2). Their specific discharges (Sect. 2.2.1) however are similar and by taking the spatiotemporal median  $v$  as an effective catchment value for each simulation the (more numerous) headwater grid cells were better represented than the grid cells close to the basin outlet. A similar effect is found for the range of the effective travel time  $TT$ . Generally these similar  $v$  and  $TT$  495 distributions from model simulations between catchments align with the notion of Langbein and Leopold (1964) that drainage networks evolve naturally to transport water (and sediment) most efficiently such that an equilibrium between channel form and water and sediment load is imposed (Leopold and Maddock, 1953). Also Damköhler numbers  $Da$  exhibited realistic ranges, mostly distributed around 1 (Oldham et al., 2013; Ocampo et al., 2006), with 36.5 % of the simulations  $< 0.8$  and 50.8 %  $> 1.2$  indicating that more simulations are reaction driven than transport driven. Finally, other variables such as the range 500 of the modelled river widths are found to be reasonable to a large degree (Fig. S4 in Supporting Information).

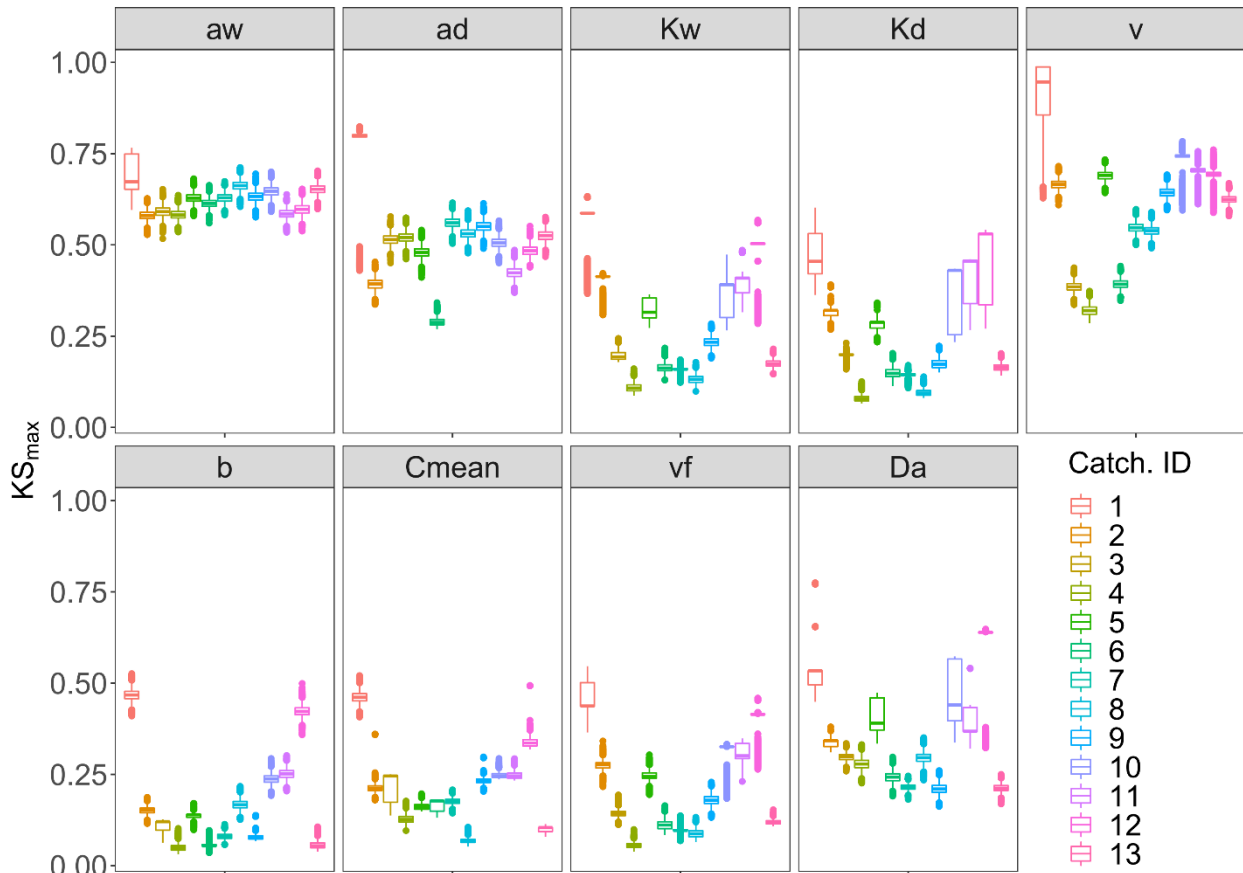
As for the simulations, the same  $>10000$  parameter input sets are applied in each catchment, differences between the catchments result from the different network structures and hydrological regimes that control transport and uptake processes for each parameter input set in each catchment. From Table 4 and Table 2 it is clear that differences in model outputs (i.e. 505  $Curv_{max}$ ,  $L_{r.perc}$  and  $Da$ ) between the catchments cannot be attributed to a single catchment property such as total network length or basin area. For example  $Curv_{max}$  has the highest variability between simulations in the smallest catchment 1, compared to the other catchments, which could be attributed to the variability in local loading and uptake patterns in the network (driven by  $Q$ ) that are still visible at the catchment outlet. Following the simulated Selke Meisdorf example in Sect. 3.1 (Fig. 3; Fig. S3), we show that  $Curv_{max}$  tends to converge to a constant value with increasing drainage areas (similar to Abbott et al., 2018 510 for nutrient concentrations, Dupas et al., 2017 for nutrient uptake and Bertuzzo et al., 2017 for DOC removal). Drainage area is however not the only catchment property influencing  $Curv_{max}$  at the outlet. For example, catchment 6 is the second largest catchment (Table 2) and has the least bent (and least variable)  $\log(C)$ - $\log(Q)$  relationships. The network structure could possibly play a role here as the largest catchment 8 has some large tributaries near the basin outlet (Fig. 1), which could bypass removal and transport high load during events, introducing a more variable  $Curv_{max}$  (Mineau et al., 2015; Helton et al., 2018). 515 The percentage load removed,  $L_{r.perc}$ , is notably lower catchments with high runoff or  $Q$  – like 3, 4 and 8 (Table 4) which corresponds with findings in Sect. 3.1 that uptake efficiency decreases with increasing  $Q$  because of increasing loads to the system (Wollheim et al., 2018; Mulholland et al., 2008) and that increasing  $Q$  results in less efficient uptake within the reactive surface area (Peterson et al., 2001; Hensley et al., 2014). The high  $L_{r.perc}$  in small catchments 1 and 10 could then be attributed to their low  $Q$ , however why the small catchment 5 does not have similar uptake performance is not evident. Generally the 520 model output variability between the catchments (as a result of different network and discharge properties) is minor compared to the output variability within the catchments (due to the effect of the chosen input parameter set).

### 3.3 $Curv_{max}$ sensitivity analysis and model parameter correlation

525 The PAWN sensitivity index  $KS_{max}$  in Fig. 4 and Table C2 shows that across all catchments  $Curv_{max}$  is most sensitive to the exponents in the width-Q relation  $a_w$  ( $KS_{max} = 0.62$ ) and depth-Q relation  $a_d$  ( $KS_{max} = 0.51$ ). Here, there is little variability between the catchments ( $KS_{max}$  has a low Coefficient of Variation, CV, of 0.06 and 0.22 respectively). Overall, the slope of the linear loading function,  $b$ , is least important in shaping  $Curv_{max}$  ( $KS_{max} = 0.14$ ). Nevertheless, a high variability of  $KS_{max}$  is observed (CV = 0.76) that is caused by larger sensitivities for catchments 1 and 12 ( $KS_{max}$  near 0.45).  $Curv_{max}$  is equally sensitive to  $v_f$  and  $C_{mean}$  ( $KS_{max}$  0.18 and 0.19) but  $v_f$  exhibits higher variability in  $KS_{max}$  than  $C_{mean}$  (CV 0.59 and 0.47).

530 Furthermore, over all the catchments  $Curv_{max}$  is sensitive to the median velocity  $v$  and the Damköhler number  $Da$  ( $KS_{max}$  equals 0.64 and 0.31 respectively, CV 0.26 and 0.38). When considering the catchments individually, basin 1 with smallest discharge has the highest median  $KS_{max}$  (0.59) across all input parameters, while catchment 4 that has the highest discharge exhibits the lowest median  $KS_{max}$  (0.13). Additionally,  $Curv_{max}$  is very sensitive to the velocity  $v$  in catchment 1 ( $KS_{max} = 0.95$ ), while it is least sensitive to  $v$  in catchment 4. Nevertheless, the other catchments show no clear order in  $Curv_{max}$

535 sensitivity according to catchment properties such as Q. For example in nested catchments 10, 11 and 12 (Fig. 1), the largest catchment 12 has the highest  $KS_{max}$  (0.50) and lowest CV (0.26) over all the input parameters, indicating that here  $Curv_{max}$  is more sensitive to the input parameters here than in the smaller sub-catchments 10 and 11.

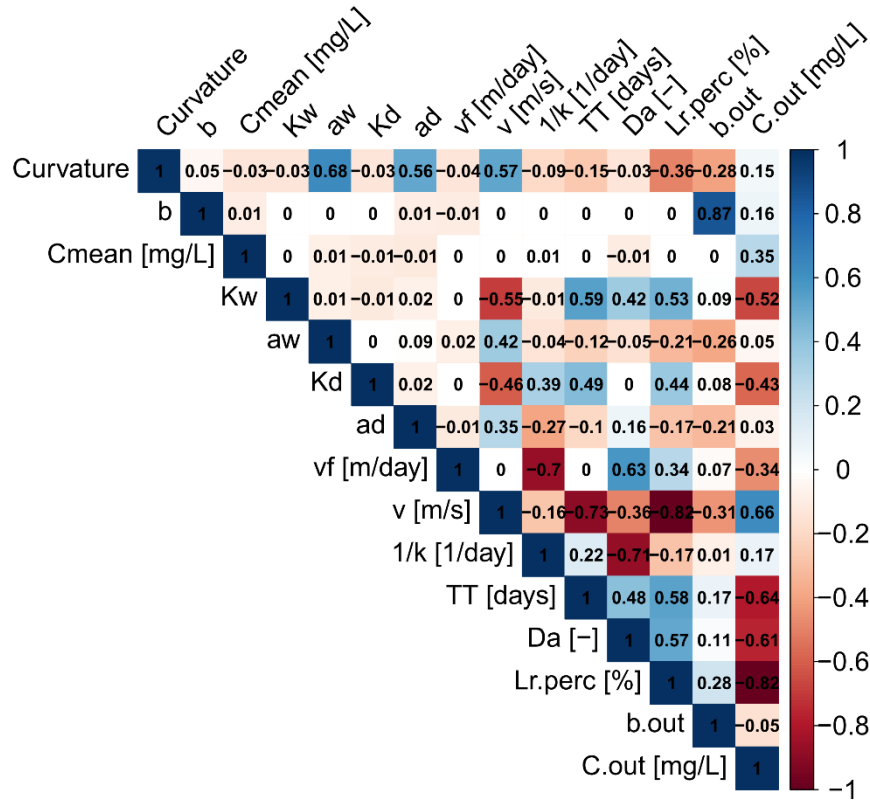


540 **Figure 4: The  $KS_{max}$  sensitivity index for each of the model input parameters and each of the 13 simulated catchments. The input parameters related to the channel geometry ( $a_d$ ,  $a_w$ ,  $K_d$  and  $K_w$ ), land-to-stream loading ( $b$  and  $C_{mean}$ ) and biogeochemistry ( $v_f$ ) are shown together with two variables derived from some of the input parameters: the median velocity  $v$  and the Damköhler number  $Da$ . Each boxplot displays 15000 bootstrapped estimates of  $KS_{max}$  for each of the 13 simulated catchments.**

In a next step the estimated  $Curv_{max}$  across all simulations is correlated to the model input parameters as well as to output variables like the percentage load removed,  $L_{r.perc}$ , the log(C)-log(Q) slope at the catchment outlet,  $b_{out}$ , the median concentration at the basin outlet  $C_{out}$  and the uptake constant  $k$ , to identify the strength and direction of their relationship. The resulting Spearman correlation matrix (Fig. 5) reflects the PAWN sensitivity findings, with the highest  $Curv_{max}$  correlation found with parameters  $a_w$  ( $\rho = 0.68$ ) and  $a_d$  ( $\rho = 0.56$ ) and input variable  $v$  ( $\rho = 0.57$ ).  $Curv_{max}$  is independent of  $v_f$  ( $\rho = -0.04$ ) but shows a negative correlation with  $L_{r.perc}$  ( $\rho = -0.36$ ), suggesting that lower  $Curv_{max}$  (more bending) is related to a higher  $L_{r.perc}$ . Furthermore,  $Curv_{max}$  is negatively correlated to the log(C)-log(Q) regression slope at the catchment outlet  $b_{out}$  ( $\rho = -0.28$ ) such that higher bending coincides with more positive  $b_{out}$ . The variable  $v$  is additionally strongly negatively correlated with  $L_{r.perc}$  ( $\rho = -0.87$ ) so high percentage load removed occurs at low velocities.  $Da$  on the other hand is positively

550

555 correlated to  $L_{r,perc}$  ( $\rho = 0.58$ ) which indicates that higher  $Da$  are occurring together with higher load removed.  $Da$ , thereby seems to be controlled more tightly by variation in  $k^{-1}$  ( $\rho = -0.71$ ) than by  $TT$  ( $\rho = 0.48$ ). Finally  $C_{out}$  is negatively correlated with  $L_{r,perc}$  ( $\rho = -0.82$ ) and  $Da$  ( $\rho = -0.61$ ).



560 **Figure 5: Correlation matrix for the model parameter inputs: channel depth and width exponents  $a_d$ ,  $a_w$  and coefficients  $K_d$ ,  $K_w$ , slope of the land-to-stream loading,  $b$ , concentration of the land-to-stream load  $C_{mean}$ , uptake velocity  $v_f$  and outputs: The bending of the log(C)-log(Q) relationship at the catchment outlet,  $Curv_{max}$ , effective stream velocity  $v$ , first order uptake constant  $k$ , travel time  $TT$ , Damköhler number  $Da$ , daily percentage load removed  $L_{r,perc}$  and slope of the log(C)-log(Q) relationship and median concentration at the outlet  $b_{out}$  and  $C_{out}$ . The Spearman rank correlation coefficients ( $\rho$ ) are given for each combination.**

The PAWN and correlation analysis results suggest the input parameters dictating the channel morphology  $a_w$  and  $a_d$  (Sect. 2.3), are controlling factors for the magnitude of the bending in log(C)-log(Q) curves at the catchment outlet. More specifically parameters  $a_w$  and  $a_d$  influence the response of the wetted perimeter ( $P_i$ , Eq. (A2)) in a given reach in the network and drive the reactive surface area ( $P_i * l_i$ ) with changes in discharge (Eq. (2.1) and (2.2); Fig. 5; Fig. B3). The absolute load removed  $L_{r,i}$  (Eq. (5)) can be written with the width and depth exponents  $a_w$  and  $a_d$  explicitly (Eq. (A3)) so that  $L_{r,i} \sim \frac{1}{Q^{1-a_w-a_d}}$ . When

the denominator is large (small  $a_w$  and  $a_d$ ) the effect of low and high Q's on the local absolute removed load increases and can lead to a lower  $Curv_{max}$  (more bending, Sect. 3.1; Fig. B6). Network based modelling studies often set the width exponent  $a_w$  to a value of 0.5 that was found to be representative for rivers globally (Bertuzzo et al., 2017; Rode et al., 2016; Wollheim et al., 2018). This a-priori fixed  $a_w$  may, however, strongly affect the simulated C-Q dynamics at the basin outlet as is demonstrated here.  $Curv_{max}$  finally shows the lowest sensitivity to the loading parameters  $b$  and  $C_{mean}$  that influence the incoming load to a grid cell (Eq. (3)) and thus impact the local absolute load removed  $L_{r,i}$  (Eq. (5)) rather than the percentage removed load  $L_{r,perc}$ . This indicates that the contribution of local incoming load in the downstream direction has a limited impact on the log(C)-log(Q) bending at the catchment outlet. For example in the Selke Meisdorf catchment, the locally contributing Q's are generally smaller (or equal for the headwaters) than the total Q in a given reach so that the influence of the loading parameters  $b$  and  $C_{mean}$  on the total load decreases in downstream reaches (Sect. 3.1; Fig. 3).

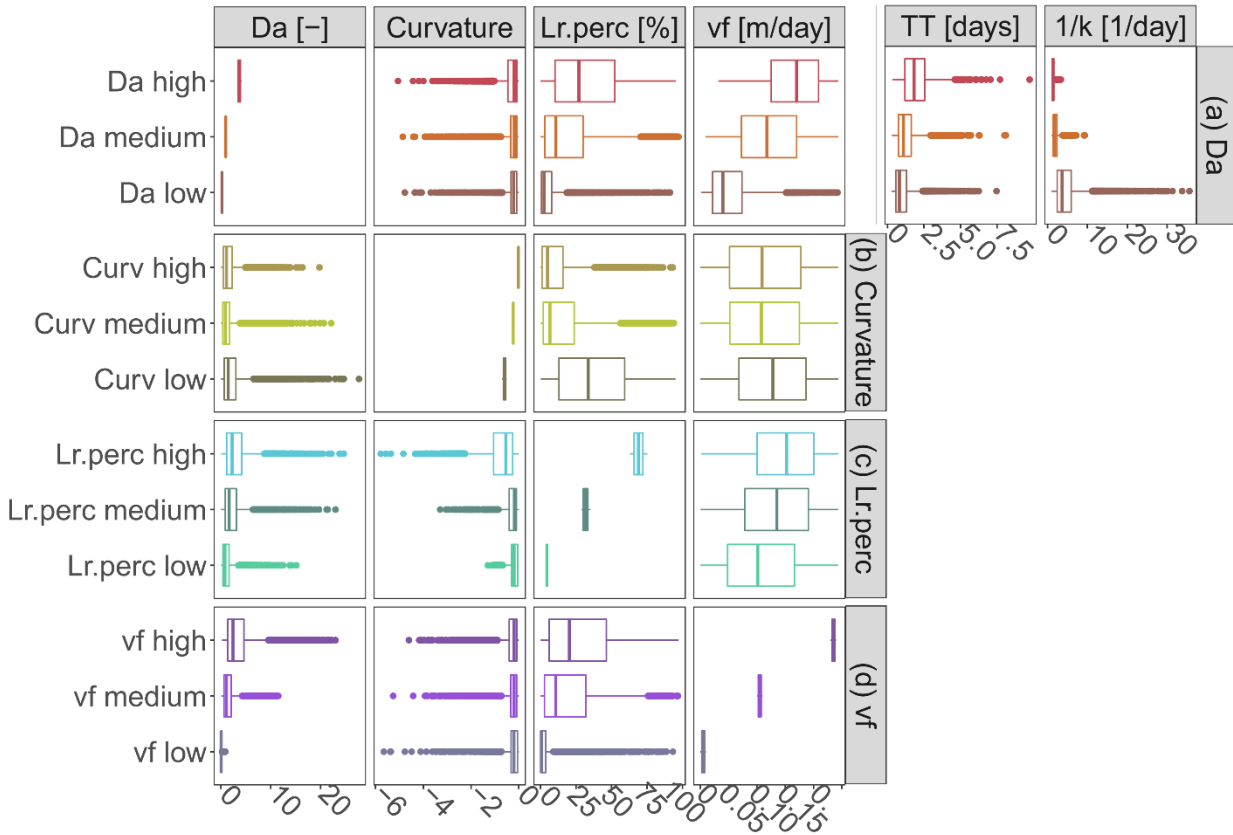
Although  $Curv_{max}$  only has an intermediate sensitivity to the uptake velocity  $v_f$  and they don't correlate well,  $v_f$  is an important 'boundary condition' for log(C)-log(Q) bending at the catchment outlet. No biological demand (low  $v_f$ ) would mean that none of the incoming load would be removed from the river network. The outlet signal would in this case be solely driven by the discharge controlled transport processes and no bending would be observed ( $Curv_{max} = 0$ ). Although increasing  $v_f$  does lead to decreasing concentrations ( $\rho = -0.34$ ) and increasing load removed ( $\rho = 0.34$ ), it does not always lead to more bending as illustrated in Fig. B6 for the Selke example. Because  $v_f$  is defined as a constant within one simulation that is independent of the local nutrient concentration (Sect. 2.2.2), the percentage of load removed in the network is mainly controlled by the varying hydrological conditions here represented by the effective network wide velocity  $v$  ( $L_{r,perc}$  and  $v$ ,  $\rho = -0.82$ ). This confirms that discharge and channel morphology are among the most important predictors of removal (Alexander et al., 2000; Seitzinger et al., 2002; Wollheim et al., 2006). The role of  $v$  was further examined in the context of restored and channelized streams (Kunz et al., 2017) and agree with our findings that decreased  $v$  influences N cycling (Peterson et al., 2001).

The PAWN and correlation analysis results show that  $Curv_{max}$  is sensitive to the Damköhler number  $Da$  ( $KS_{max} = 0.31$  Fig. 4, Table C2) that has a high positive correlation with the percentage load removed  $L_{r,perc}$  ( $\rho = 0.58$ ; Fig. 5). This indicates that high  $Da$  occur concurrently with more efficient removal and is in line with others (Ocampo et al., 2006) who found sometimes almost 100 %  $\text{NO}_3^-$  removal in the riparian zones of an agricultural catchment with  $Da$  exceeding 2. The transport timescale  $TT$  that makes up  $Da$  ( $\rho = 0.48$ ; Fig. 5) together with the inverse of the first order uptake constant  $k^{-1}$  ( $\rho = -0.71$ ; Eq. (6)) are examined for classes of low, median and high  $Da$  (defined in Table 3) in Fig. 6a to disentangle which values of  $k^{-1}$  and  $TT$  occur together and can constitute a certain  $Da$  range (each class contains 5 % of all simulations). It is shown here that low  $Da$  are driven by both low  $TT$  and high, variable  $k^{-1}$  implying a transport driven system with limited  $\text{NO}_3^-$  removal (median  $L_{r,perc}$  equals 2.4 % in Fig. 6a for low  $Da$ ). High  $Da$ , contrarily, have high  $TT$  and low  $k^{-1}$ , fostering intermediate uptake percentages (median  $L_{r,perc} = 27.1$  %). Although also  $v_f$  clearly differentiates for classes of low, medium and high  $Da$

in Fig. 6a, the corresponding  $Curv_{max}$  values are similar in their range and mean. Nevertheless, this does not mean that  $Da$  is not influencing  $Curv_{max}$  at the basin outlet as there could be interactions with other inputs that are not captured here (which is supported by the PAWN findings, where  $Da$  appears to be influential).

605 From the  $Curv_{max}$  perspective (Fig. 6b) we identify model output ranges of  $L_{r.perc}$ ,  $Da$  and input variable  $v_f$  that constitute low, median and high  $Curv_{max}$  classes (Table 3). High  $Curv_{max}$  (less bending,  $\sim -0.02$ ) is thereby linked to low  $L_{r.perc}$  (median 4.8 %), while low  $Curv_{max}$  (more bending,  $\sim -0.60$ ) is connected to higher and more variable  $L_{r.perc}$  (median 33.6 %), generally indicating that more bent systems are more efficient in terms of removal and vice-versa. To explore some cases when this latter statement might not be true, we examine the input parameter ranges where more bent simulations ( $Curv_{max} < -0.51$ , 13.1 % of  
610 all simulations) occur concurrently with low percentage removal ( $L_{r.perc} < 5.2$  %, 0.9 % of all simulations) on the one hand and high percentage removal ( $L_{r.perc} > 63.0$  %, 4.9 % of all simulations) on the other hand in Fig. B7a. Here, it is seen that high bending, low uptake cases mainly occur for simulations with a high effective velocity  $v$  (driven by lower values for the channel shape parameters  $K_w$ ,  $K_d$ ,  $a_w$  and  $a_d$ ). As discussed before, low  $a_w$  and  $a_d$  are correlated with more bending (low  $Curv_{max}$ ) and  $Curv_{max}$  is most sensitive to these parameters. However, we show here that these low  $a_w$  and  $a_d$  do not lead to a  
615 more efficient  $\text{NO}_3^-$  uptake if the other channel shape parameters cause relatively high velocities (median  $v > 0.1$  m s<sup>-1</sup>), throughout the network. Although the latter case is shown to be true for a minor percentage of all simulations (0.9 %), it still explains why low  $Curv_{max}$  (more bending) can be connected to a wider range of  $L_{r.perc}$ . A similar analysis in Fig. B7b for less bending ( $Curv_{max} > -0.03$ ) shows that concurrent high removal simulations ( $L_{r.perc} > 63.0$  %) are even rarer (0.1 % of all simulations) compared to concurrent low removal ( $L_{r.perc} > 5.2$  %; 7.4 % of all simulations). Deviations from the expected  
620 'high  $Curv_{max}$  - low  $L_{r.perc}$  pattern are also here driven by (very low)  $v$ . In this case however,  $a_w$  and  $a_d$  are generally high in both cases (leading to high  $Curv_{max}$ ) and the different  $v$  stem from coefficients  $K_w$  and  $K_d$  that are higher in high removal simulations. Finally, Fig. 6d illustrates that low medium and high uptake velocities  $v_f$  lead to distinct  $Da$  and  $L_{r.perc}$  but do not show up in the bent signal at the catchment outlet.





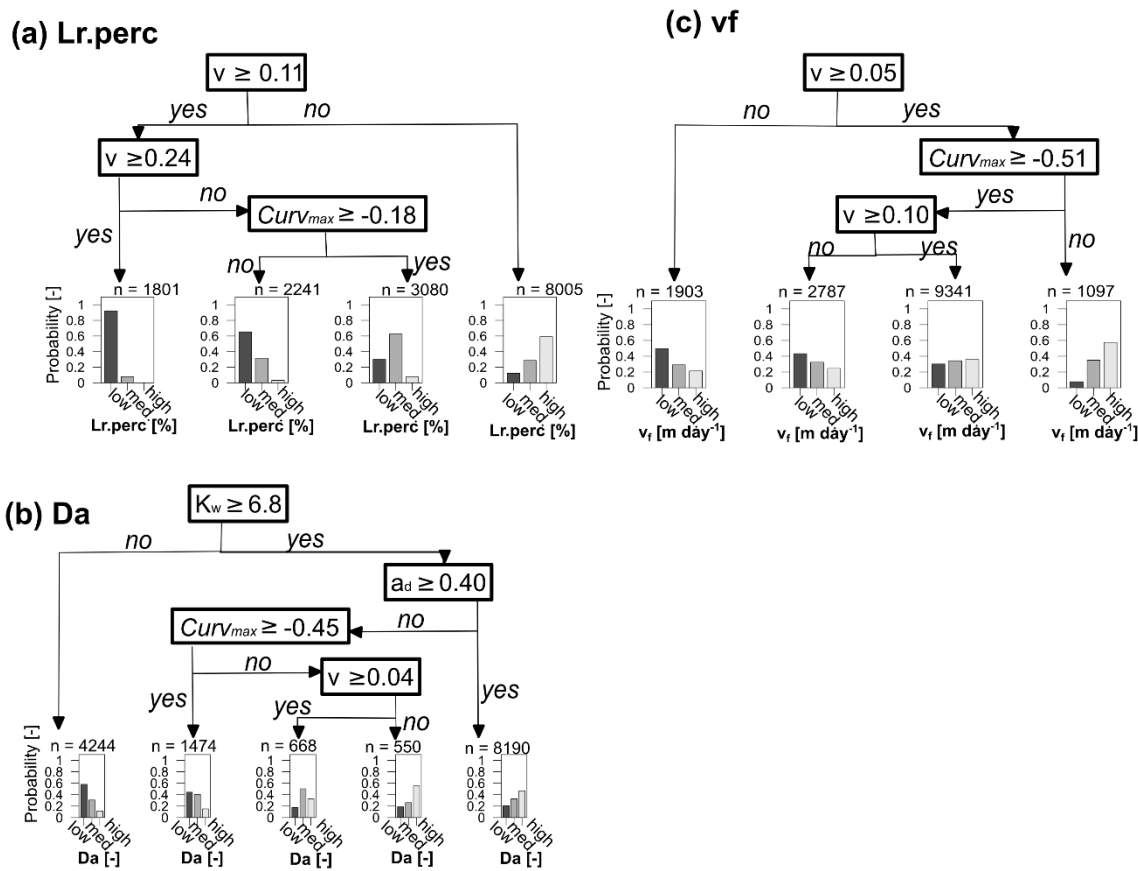
625 **Figure 6: The corresponding simulated ranges for high, median and low values (Table 3) of the main simulation outputs: (a) Damköhler number  $Da$ , (b)  $Curv_{max}$ , (c) Percentage load removed  $L_{r.perc}$  and (d) uptake velocity  $v_f$  are shown for the same variables (in the columns). The median travel time,  $TT$ , and the inverse of the first order uptake constant,  $k^{-1}$  are given additionally for low medium and high  $Da$ .**

### 630 3.4 Predicting in-stream processing with $Curv_{max}$

To determine if observed C-Q bending at the catchment outlet (here  $Curv_{max}$ ) can be utilized to quantify in-stream uptake in the upstream river network and to visualize model parameter interactions, a classification tree was established for low, medium and high values (Table 3; Fig. 6) of the response variables  $L_{r.perc}$ ,  $Da$  and  $v_f$  (Fig. 7). The prediction accuracy metrics in Table C3 and the probability histograms in Fig. 7 show that  $L_{r.perc}$  can be predicted relatively well (overall accuracy of 0.66) compared to the other response variables  $Da$  (accuracy 0.51) and  $v_f$  (accuracy 0.40). The fitted CART models all perform significantly better than a random allocation of simulation results to each class for each response variable (Accuracy > No Information Rate, p-value < 2.2e-16). While the classes for  $L_{r.perc}$  and  $v_f$  are partitioned using only the network effective velocity  $v$  and  $Curv_{max}$ , predicting  $Da$  in our case requires information on the channel geomorphology parameters the width coefficient  $K_w$  and the depth exponent  $a_d$ . The histograms for each of the response variables in Fig. 7 indicate the probability

635

640 of a test sample to be of a certain class when following the partition rules in the respective decision tree. For example, for  $L_{r.perc}$  the probability that the daily percentage load removed is small (around 8%) exceeds 0.95 when the effective velocity  $v$  in the catchment is larger than  $0.22 \text{ m s}^{-1}$ ; while the probability that  $L_{r.perc}$  is high (around 70%) in this case is close to 0 (Fig. 7a). For  $v_f$  the lowermost (1) and highest (20) classes are predicted most accurately (0.58 and 0.56 respectively, Table C3) and indicate that when the velocity is not very small and  $Curv_{max}$  is smaller than  $-0.51$  (more bent),  $v_f$  is most likely high (probability 0.59). For  $Da$ , the lower and higher classes can be predicted most accurately (0.69 and 0.68 respectively), for example,  $Da$  is small with a probability of 0.58 when  $K_w$  is relatively low ( $< 6.8$ ). When on the other hand  $K_w$  exceeds 6.8 and  $a_d$  is larger than 0.4 or when  $a_d$  is smaller than 0.4 but  $Curv_{max}$  is smaller than  $-0.45$  and  $v$  is very small ( $< 0.04 \text{ m s}^{-1}$ ) it is most likely that  $Da$  is large.



650

**Figure 7: CART decision trees for the response variables  $L_{r.perc}$  (accuracy = 0.66),  $Da$  (accuracy = 0.51) and  $v_f$  (accuracy = 0.40). The histograms illustrate the probability of a test sample to be from a certain response variable class (low, medium or high; Table 3) when following the binary splits of the decision tree. The variables at the binary splits differ per response variable and consist of the median stream velocity,  $v$  [ $\text{m day}^{-1}$ ] and  $Curv_{max}$  for response variables  $L_{r.perc}$  and  $v_f$ , while width coefficient  $K_w$  and depth**

655 exponent  $a_d$  are identified additionally for  $Da$ . The prediction metrics for each of these classes and response variables are stated in Table C3.

These findings demonstrate that  $\log(C)$ - $\log(Q)$  bending at the catchment outlet, together with the median velocity and the response of the width and the depth of a channel to discharge (parameters  $K_w$ ,  $K_d$ ,  $a_w$  and  $a_d$ ) can help to classify the in-stream  
660 daily percentage load removed  $L_{r.perc}$ , the Damköhler number  $Da$  and to a certain extent the uptake velocity  $v_f$ . This conclusion depends of course on the initial assumptions of our model setup (e.g. linear land-to-stream loading vs  $Q$  with a constant slope  $b$  and no dominant influence of waste water sources, no seasonality in uptake velocity  $v_f$ ). The velocity may be computed from the channel shape, discharge (Eq. (2.3)) and the topography with the channel shape parameters that are sometimes available from rating curve information or detectable from high resolution satellite pictures. The CART models  
665 could help obtain an initial probability of  $\text{NO}_3^-$  removal efficiency in a river network, especially in a context where network wide uptake measurements are scarce (Wollheim et al., 2017; Hensley et al., 2014) and physical, fully distributed models are not always feasible to apply (Boyer et al., 2006; Klemes, 1986). Although the CART models are developed using ‘only’ the 13 German catchments included in the Monte Carlo analysis, in Sect. 3.2 and Table 4 we have shown that the output variability between the catchments (as a result of different catchment properties) is minor compared to the output variability within the  
670 catchments (due to the effect of the input parameter set) thus justifying the CART model use. Nevertheless, the prediction performance of these CART models might be influenced in unknown ways when applied to catchments with dissimilar catchment sizes, network structures or hydrological regimes.

#### 4 Conclusions

675 In this study, we explore how low frequency  $\text{NO}_3^-$   $\log(C)$ - $\log(Q)$  relationships, observed at a basin outlet, can display bending as a result of network scale in-stream uptake processes. We established a parsimonious grid based river network model for 13 distinct German catchments and investigated the influence of in-stream loading, transport and uptake parameters on the bending of  $\log(C)$ - $\log(Q)$  relationships. Based on our exploratory analysis we conclude that:

- 680 • Noisy, multi-annual and low frequency  $\text{NO}_3^-$   $\log(C)$ - $\log(Q)$  relationships at a basin outlet can be described as bent and the amount of bending can be robustly quantified with the new  $Curv_{max}$  metric.  $Curv_{max}$  is temporally stable on multi-annual time scales and can be computed alongside existing  $\log(C)$ - $\log(Q)$  descriptors, such as the slope of the linear regression model.
- 685 • A bent  $\log(C)$ - $\log(Q)$  relationship ( $Curv_{max} < 0$ ) at the basin outlet can arise from  $\log$ - $\log$  linear land to stream C-Q relationships and if uptake is present within the river network. This supports the hypothesis that more positive slopes under low flow (bended  $\log(C)$ - $\log(Q)$  curves) are linked to biological  $\text{NO}_3^-$  concentration mediation in the stream (Moatar et al., 2017); and connects  $Curv_{max}$  (as a quantitative measure) to observations of increased removal efficiency

under low flows (Wollheim et al., 2017). This also stresses the need to monitor the entire discharge range and capture low flows as well as high flows in a catchment.

- The bending at the catchment outlet is primarily shaped by the channel geomorphological parameters,  $a_w$  and  $a_d$  (exponents in the respective stream width and depth to discharge relationships; with  $Curv_{max}$  sensitivity indices  $KS_{max}$  equal to 0.62 and 0.51; and Spearman correlation coefficient,  $\rho$ , equaling 0.68 and 0.56 respectively) and less by the uptake velocity  $v_f$  ( $KS_{max} = 0.18$ ,  $\rho = -0.04$ ), given that  $v_f$  differs from zero. In that case  $Curv_{max}$  would equal zero and the log(C)-log(Q) relationship would be solely shaped by the accumulation of upstream load. Thus, the change of reactive channel bed area with discharge (mediated by  $a_w$  and  $a_d$ ) has a greater influence on the bending at the outlet than the biological removal capacity (here  $v_f$ ). Additionally we demonstrate that an a-priori fixed  $a_w$  might strongly affect the simulated C-Q dynamics at the basin outlet. This calls for a better representation of channel geomorphological parameters at stream networks to allow for better modeling assessments.
- $Curv_{max}$  at the basin outlet can be linked to the network-wide removal efficiency  $L_{r.perc}$  ( $\rho = -0.36$ ), indicating that systems with more bending in their log(C)-log(Q)-relationship are more efficient in terms of removal and vice-versa. It is, however, clear that also cases with high bending ( $Curv_{max} < -0.51$ ) and low removal ( $L_{r.perc} < 5.2\%$ , 0.9% of all simulations) or low bending ( $Curv_{max} > -0.03$ ) with high removal ( $L_{r.perc} > 63.0\%$ , 0.1% of all simulations) exist that are imposed by respective higher and lower network wide median velocities. This shows how the velocity,  $v$ , (calculated from the channel shape parameters  $a_w$ ,  $a_d$ ,  $K_w$  and  $K_d$ ) may mediate the connection between  $L_{r.perc}$  and  $Curv_{max}$  and stresses that  $v$  should be considered when interpreting log(C)-log(Q) bending. Consequently, anthropogenic impacts in terms of channelization of river networks might lead to lower removal efficiencies.
- Simple classification trees - like CART - can be useful for predicting low, median and high classes of response variables  $L_{r.perc}$ , the Damköhler number  $Da$  and  $v_f$ . They provide useful insights on how catchments with low frequency concentration and discharge time series (that are generally available) can reveal information on the upstream river network uptake performance.

To evaluate the generality of the results presented here,  $Curv_{max}$  should be calculated for  $\text{NO}_3^-$  concentration observations of a larger range of catchments and linked to the respective catchment properties. Properties such as light and stream ecological state can serve as proxies for uptake performance and for example topographic gradient can be a proxy for network transport velocity. Such a data-driven exploration would further elucidate the linkages between nutrient uptake efficiency and low-frequency C and Q observations.

## Appendix A

c calculation (Jawitz and Mitchell, 2011)

$$c = e^{\mu_c - b * \mu_q} \quad (\text{Eq. A1})$$

720 With

$$\mu_q = \text{mean}(\log Q_{t.sp} * a_i)$$

$$\mu_c = \log \text{mean} C - \frac{\sigma_c^2}{2}$$

$$\sigma_c = \sqrt{b^2 * \sigma_q^2}$$

$$\sigma_q = \sqrt{\text{var}(\log Q_{t.sp} * a_i)}$$

725

Stream channel wetted perimeter  $P_i$  [L], where  $A$  is the cross-sectional area [L<sup>2</sup>],  $R_H$  [L] is the hydraulic radius and  $w_i$  [L],  $d_i$  [L] and  $v_i$  [L/T] are the local stream width, average depth and velocity respectively.  $S_i$  [L/L] is the stream bed slope and  $n$  [-] is the Manning roughness coefficient that is equal to 0.03 for all simulations.

$$P_i = \frac{A}{R_H} = \frac{w_i * d_i * S_i^{\frac{3}{2}}}{(v_i * n)^{\frac{3}{2}}} \quad (\text{Eq. A2})$$

730

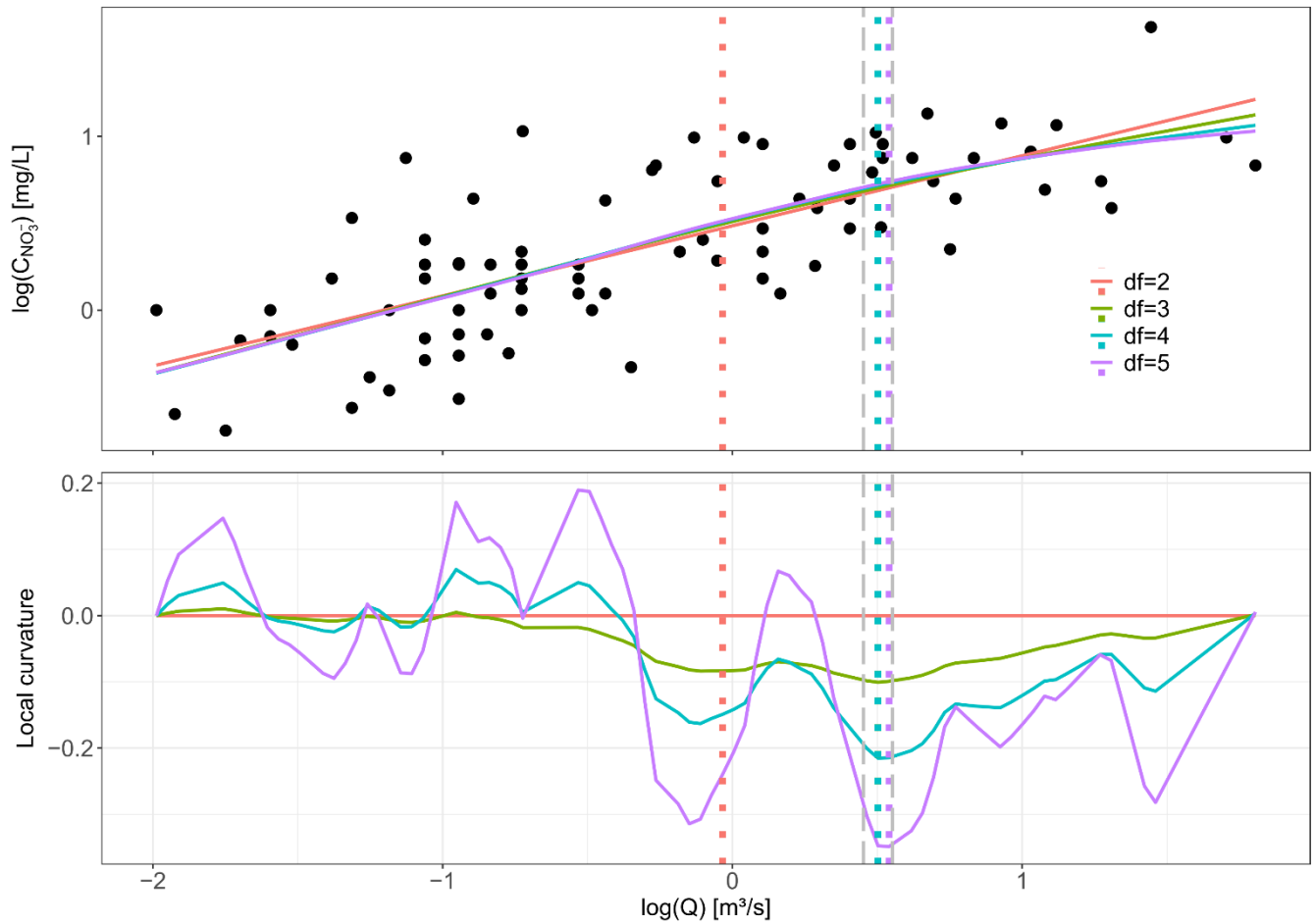
The load removed in a grid cell (Eq. (5)) with the width and depth exponents,  $a_w$  and  $a_d$ , stated explicitly.

$$L_{r,i} = L_{in,i} * \left( 1 - e^{-\frac{v_f * (K_w * K_d)^{\frac{5}{2}} * S_i^{\frac{3}{2}} * n^{\frac{3}{2}}}{Q_i^{1-a_w-a_d}}} \right) \quad (\text{Eq. A3})$$

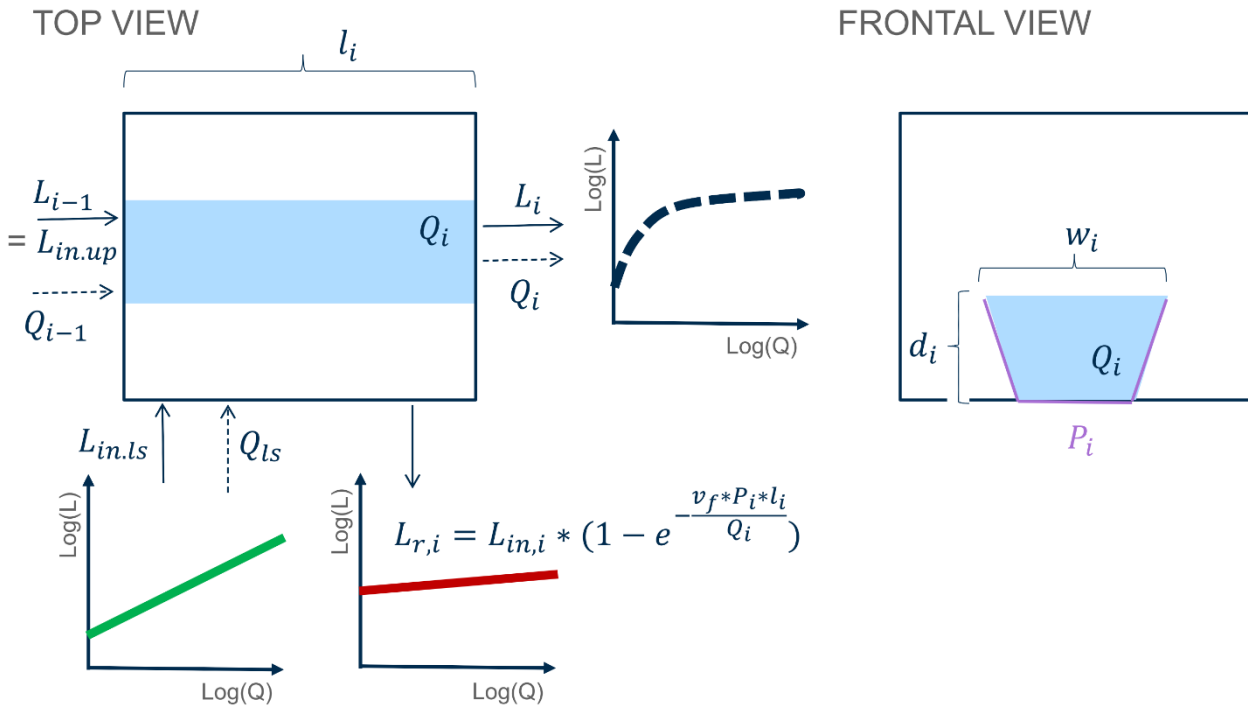
The velocity in a grid cell (Eq. (2.3)) with the width and depth exponents,  $a_w$  and  $a_d$ , stated explicitly.

$$735 \quad v_i = \frac{Q^{1-a_w-a_d}}{K_w * K_d} \quad (\text{Eq. A4})$$

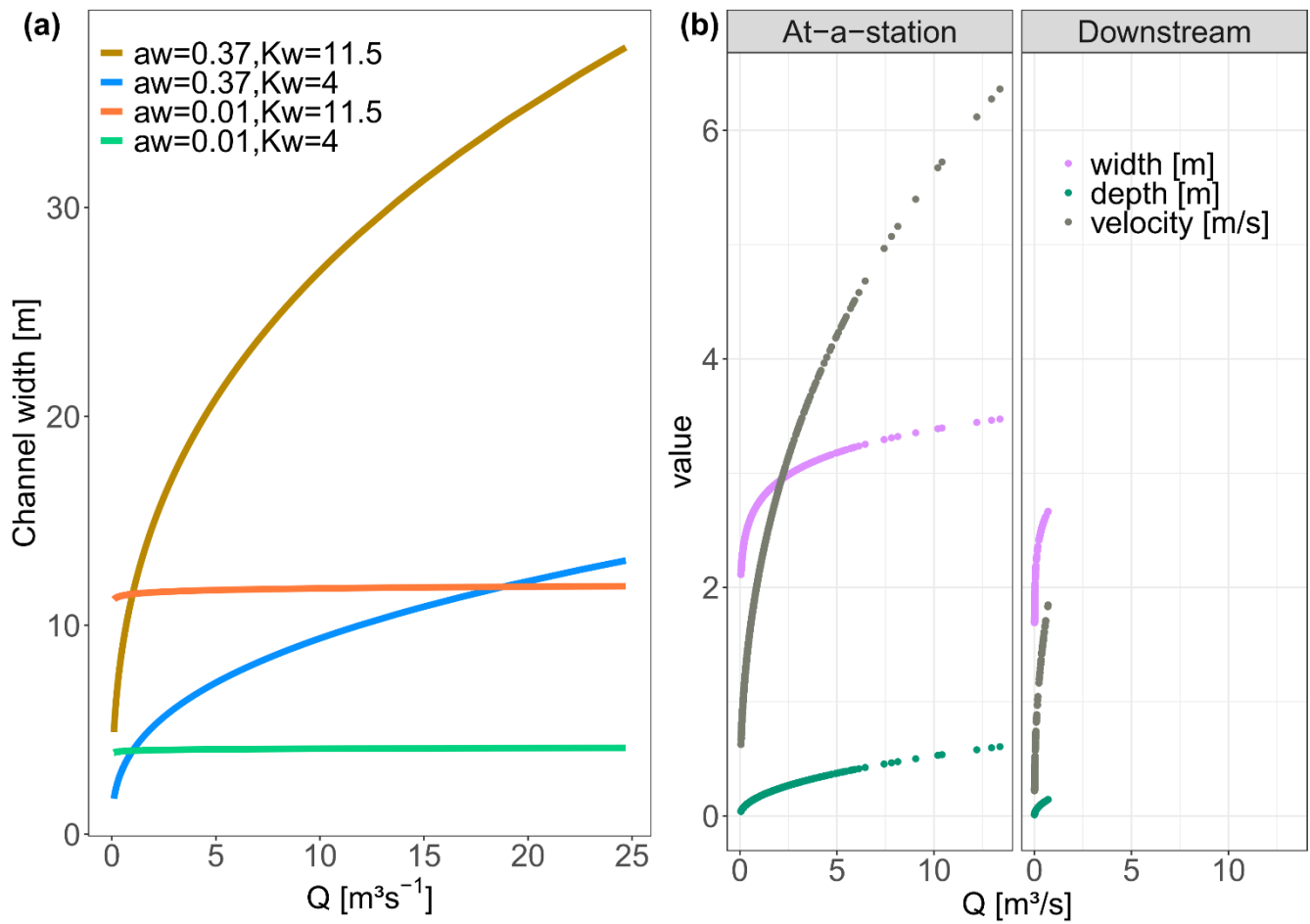
## Appendix B



740 **Figure B1: Conceptual figure explaining  $Curv_{max}$ .** The upper panel shows the  $\log(C)$ - $\log(Q)$  relationship for Selke Meisdorf with the  
 smoothed spline fits to this data for different degrees of freedom (df). The corresponding colors in the lower plot show then the local  
 745 curvature values for these fitted smoothed spline. Also the  $\log(Q)$  is indicated for which the largest local curvature was found for  
 each of the smoothed splines.  $Curv_{max}$  is then calculated as the largest local curvature value for a certain degree of freedom. Note  
 that when  $Curv_{max} < 0$  the curve is concave while for  $Curv_{max} > 0$  the curve is convex.

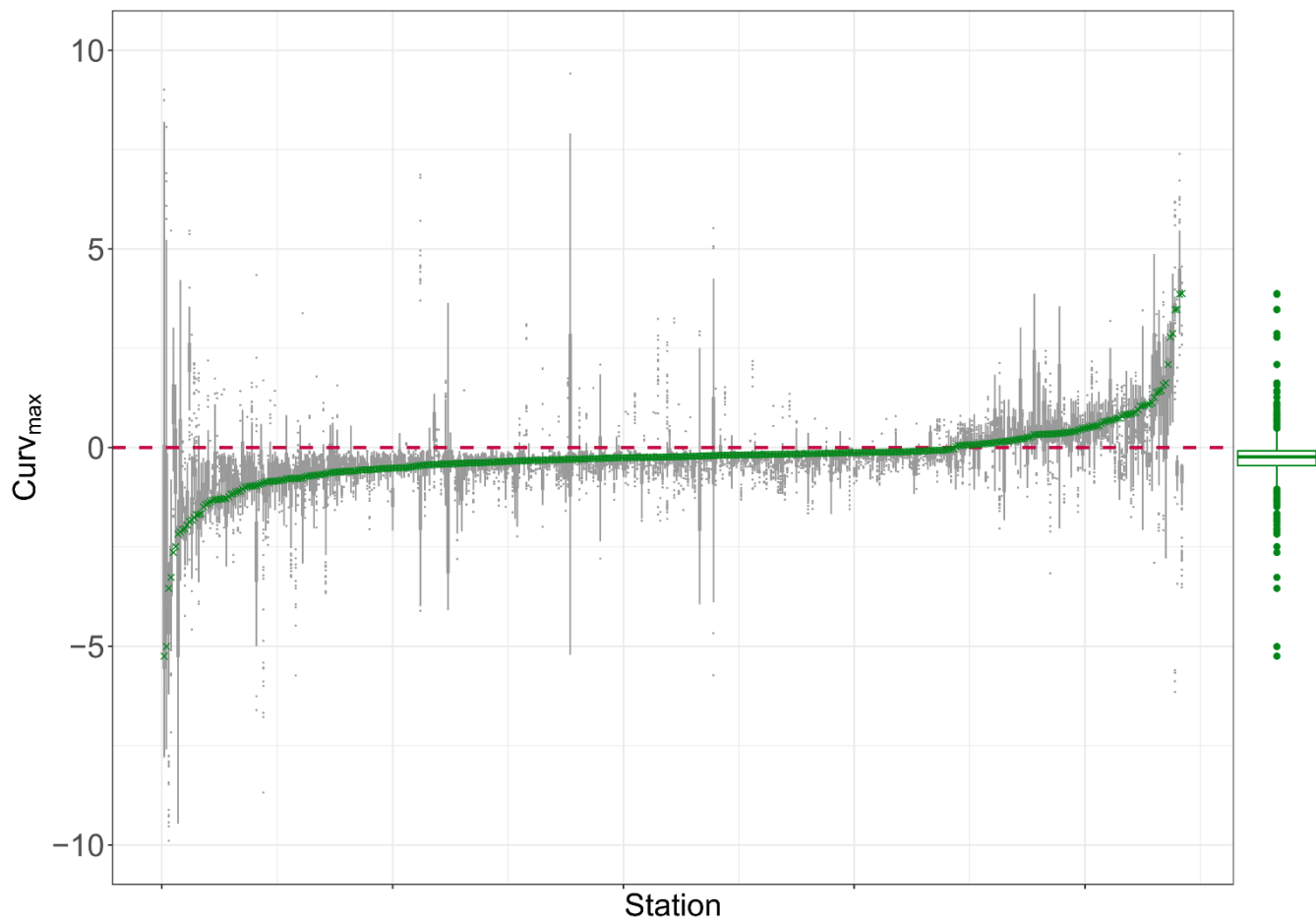


750 **Figure B2: Network model, illustrated for one grid cell.** Here, the flow length through a grid cell  $i$  is  $l_i$  [L],  $w_i$  [L] and  $d_i$  [L] are the respective width and average depth of the reach and  $P_i$  [L] is the corresponding stream channel wetted perimeter. The uptake velocity is denoted as  $v_f$ . The local discharge  $Q_i$  [ $L^3 T^{-1}$ ] consists of upstream incoming discharge  $Q_{i-1}$  [ $L^3 T^{-1}$ ] and land to stream runoff  $Q_{ls}$  [ $L^3 T^{-1}$ ]. Similarly, the local load  $L$  [ $M T^{-1}$ ] consists of upstream incoming load  $L_{in.up}$  [ $M T^{-1}$ ] and the land to stream load  $L_{in.ls}$  [ $M T^{-1}$ ], where  $L_{in.} = L_{in.up} + L_{in.ls}$ . Finally, the local load removed is denoted as  $L_{r,i}$  [ $M T^{-1}$ ].

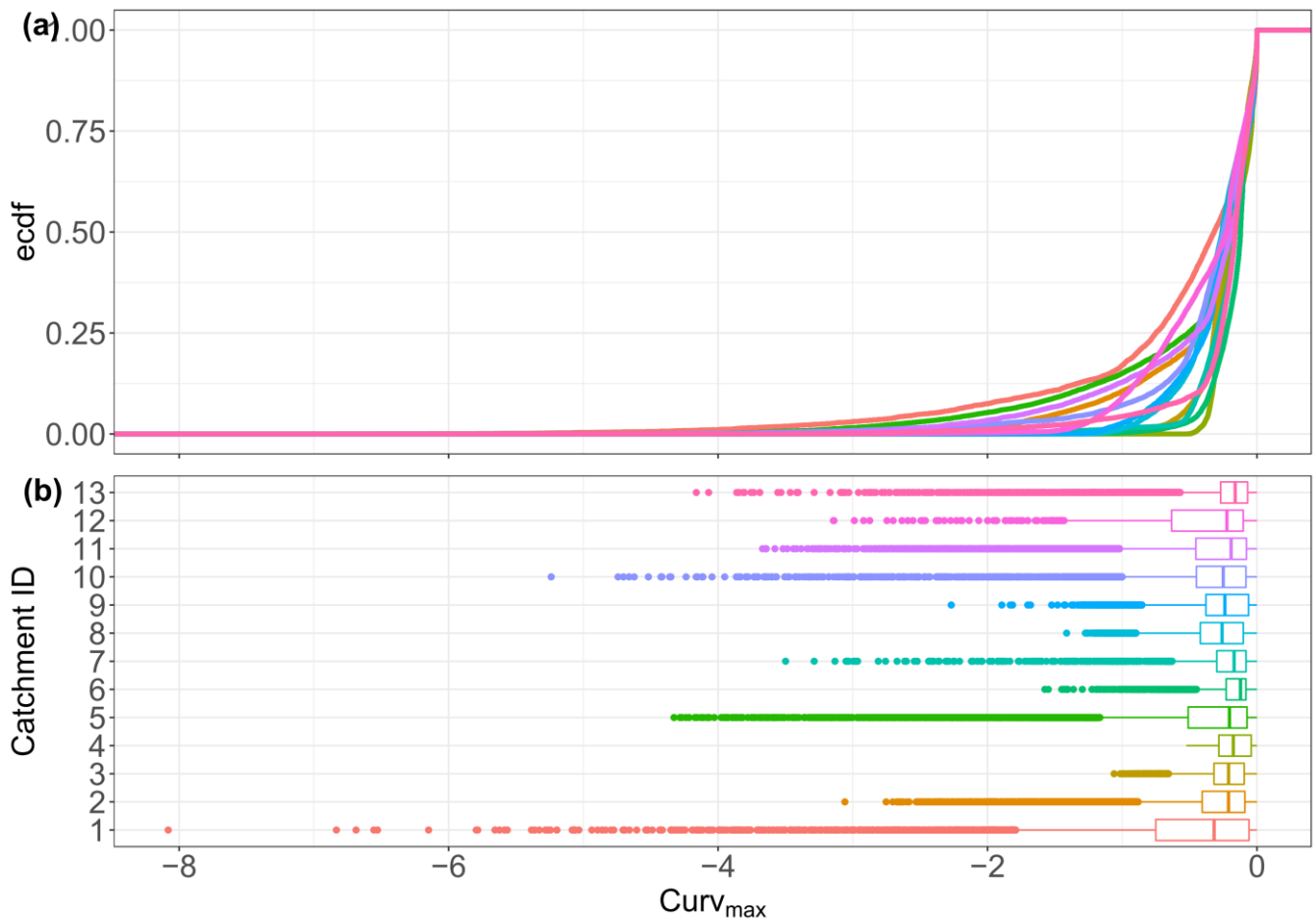


755 **Figure B3:** (a) The effect of parameters  $a_w$  and  $K_w$  on the channel width illustrated for the  $Q$  timeseries at the Selke Meisdorf station. (b) In the ‘At-a-station’ panel the changes in velocity, depth and width with  $Q$  for grid cell B (Fig. 3) in the middle of the Selke network are evaluated. The ‘Downstream’ panel - that considers all the network grid cells - shows the channel characteristics width, depth and velocity for a time  $t$ , with a  $Q$  of  $0.70 \text{ m}^3 \text{ s}^{-1}$  at the outlet. The values for the parameters  $a_w$ ,  $K_w$ ,  $a_d$  and  $K_d$  are the same for both scenarios (Table C1).

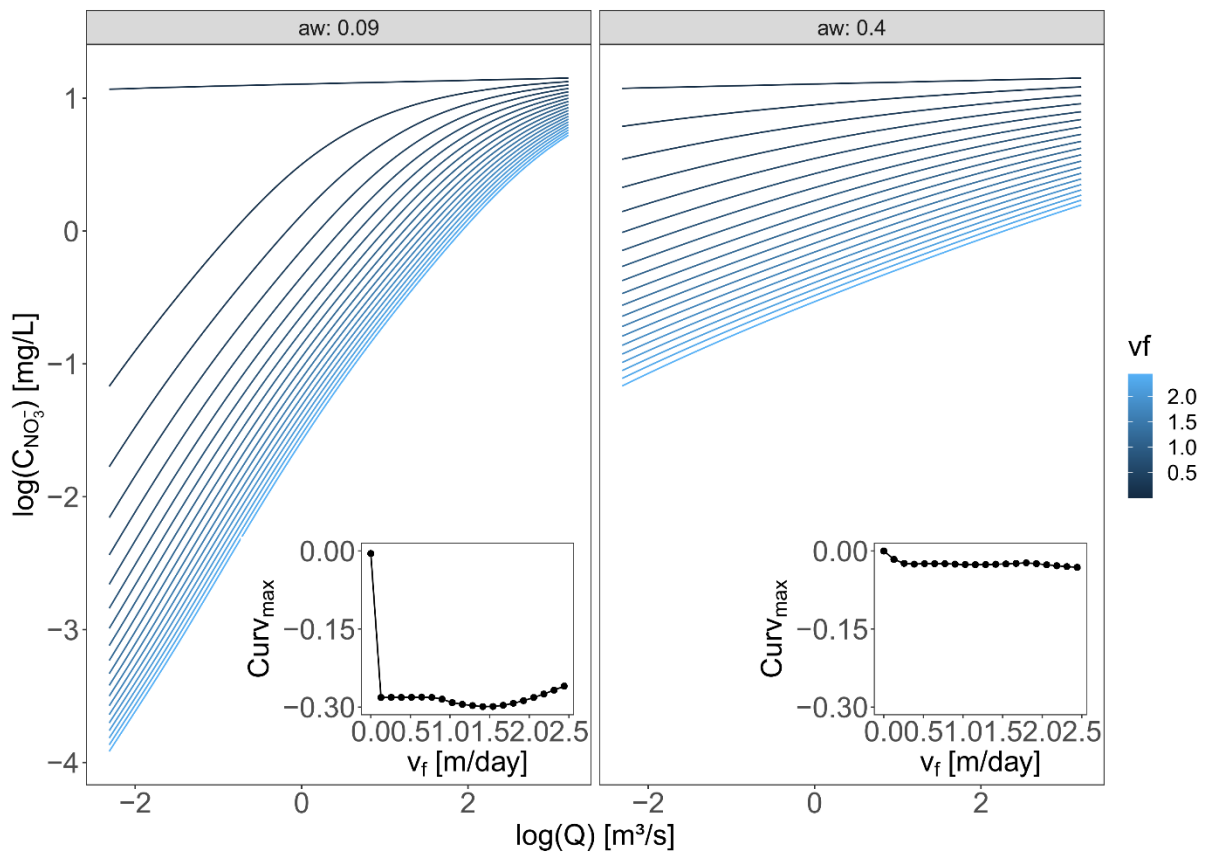




760 **Figure B4:**  $Curv_{max}$  of nitrate  $\log(C)$ - $\log(Q)$  data for 444 French monitoring stations arranged from left to right with increasing  $Curv_{max}$  (green crosses). For a given station, the grey boxplot represents the temporal robustness of this metric by subsampling 100 times from the original time series. The green boxplot indicates the range and distribution of all observed station  $Curv_{max}$  values.





765 **Figure B5:**  $Curv_{max}$  distributions resulting from running the same 11107 input parameter combinations in each of the 13 catchments (a) shows the elemental cumulative distribution and (b) boxplots. None of the catchments have a normally distributed  $Curv_{max}$  set according to the Kruskal-wallis ( $p < 0.05$ ) test.





770 **Figure B6: Log(C)-log(Q) relationships and  $Curv_{max}$  for increasing uptake velocities ( $v_f$ ) resulting from network model simulations of the Selke Meisdorf catchment. As an example, two different  $a_w$  are displayed and  $v_f$  is varied from almost 0 to 2.5 m day<sup>-1</sup> with the other parameter values as stated in Table C1.**

775

780

**(a)**  Curv low Lr.perc high  Curv low Lr.perc low

**(b)**  Curv high Lr.perc high  Curv high Lr.perc low

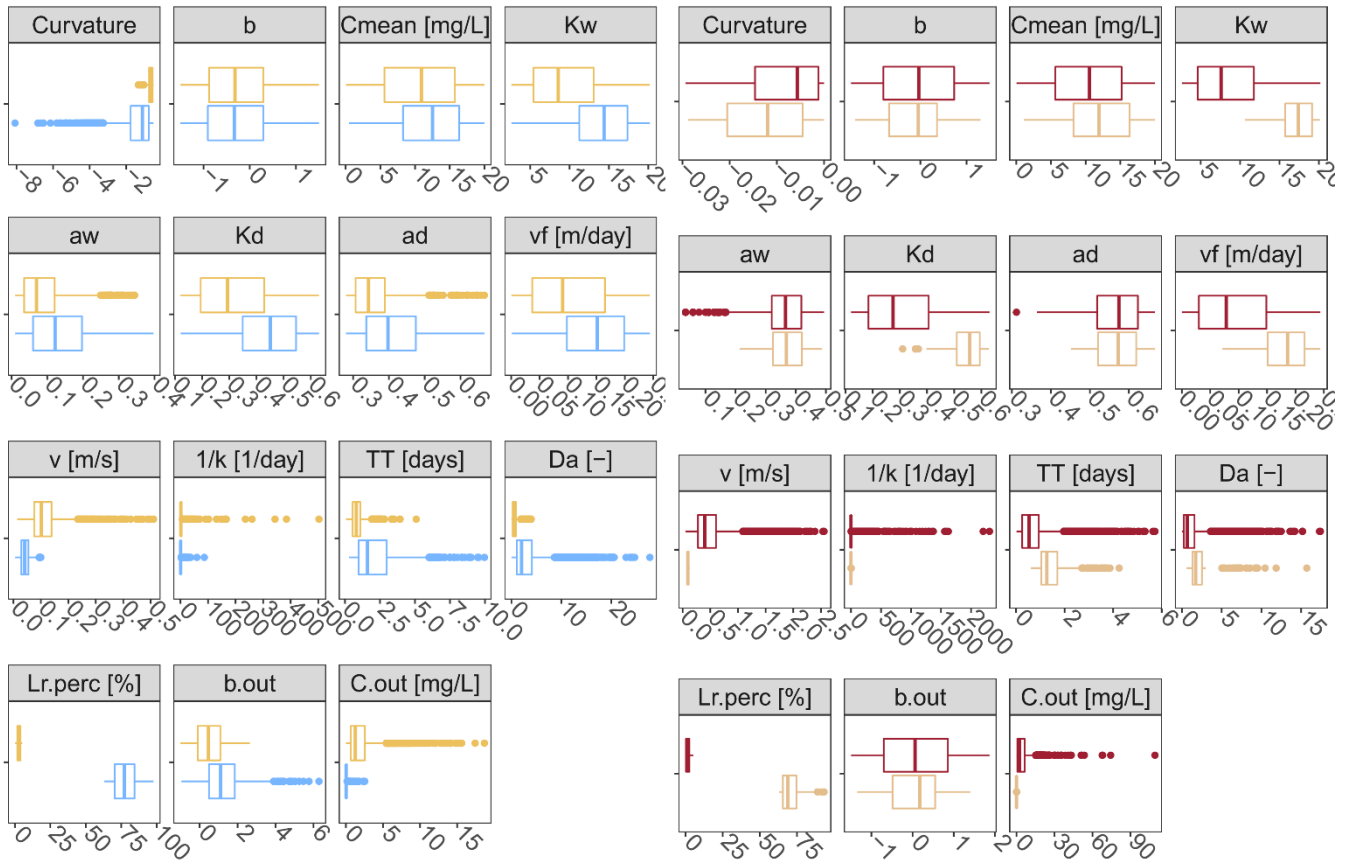


**Figure B7:** Two specific cases of Fig. 6, (a) when  $Curv_{max}$  is low (high bending) and  $Lr.perc$  is low opposed to high and (b) when  $Curv_{max}$  is high (low bending) and  $Lr.perc$  is high opposed to low.

## Appendix C

**Table C1: Estimated parameter values for the Selke catchment**

Parameter	Validation Value Selke
$v_f$	0.098
$b$	0.014
$C_{mean}$	3.014
$K_w$	2.75
$a_w$	0.09
$K_d$	0.17
$a_d$	0.49

**Table C2: PAWN sensitivity indices  $KS_{max}$  for all the parameters and all the catchments, together with median and coefficients of variation (CV).**

Parameter	Catchment ID														Median	CV
	1	2	3	4	5	6	7	8	9	10	11	12	13			
$v_f$	0.44	0.28	0.14	0.06	0.24	0.11	0.10	0.09	0.18	0.33	0.30	0.41	0.12	0.18	0.59	
$b$	0.47	0.15	0.12	0.05	0.14	0.05	0.08	0.17	0.08	0.24	0.25	0.42	0.05	0.14	0.76	
$C_{mean}$	0.46	0.21	0.25	0.13	0.16	0.18	0.18	0.07	0.23	0.25	0.25	0.34	0.10	0.19	0.47	
$K_w$	0.59	0.41	0.19	0.11	0.32	0.16	0.16	0.13	0.23	0.39	0.41	0.50	0.17	0.23	0.51	
$a_w$	0.75	0.58	0.59	0.58	0.63	0.61	0.63	0.66	0.63	0.65	0.58	0.60	0.65	0.62	0.06	
$K_d$	0.45	0.32	0.20	0.08	0.29	0.15	0.14	0.09	0.17	0.46	0.43	0.53	0.16	0.20	0.55	
$a_d$	0.80	0.39	0.52	0.52	0.48	0.29	0.56	0.53	0.55	0.51	0.42	0.48	0.53	0.51	0.22	
<b>Median</b>	0.59	0.39	0.25	0.13	0.33	0.18	0.18	0.17	0.24	0.43	0.42	0.50	0.18			
<b>CV</b>	0.31	0.46	0.53	0.81	0.53	0.65	0.67	0.76	0.58	0.45	0.41	0.26	0.74			
<b>Variable</b>																
$Da$	0.53	0.34	0.30	0.28	0.39	0.24	0.22	0.30	0.21	0.44	0.37	0.64	0.21	0.31	0.38	
$v$	0.95	0.67	0.39	0.32	0.69	0.39	0.55	0.54	0.64	0.74	0.70	0.69	0.62	0.64	0.26	

**Table C3: Performance statistics for each of the classes for the variables  $L_{r,perc}$ ,  $Da$  and  $v_f$  predicted by CART.**

	$L_{r,perc}$			$v_f$			$Da$		
	class 7	class 12	class 18	class 1	class 10	class 20	class 3	class 10	class 18
<b>Sensitivity</b>	0.63	0.38	0.94	0.43	0.00	0.77	0.63	0.07	0.82
<b>Specificity</b>	0.91	0.89	0.69	0.74	1.00	0.36	0.75	0.97	0.54
<b>Pos Pred Value</b>	0.77	0.62	0.61	0.45	NA	0.38	0.56	0.54	0.47
<b>Neg Pred Value</b>	0.83	0.75	0.96	0.72	0.67	0.76	0.80	0.68	0.86
<b>Prevalence</b>	0.34	0.32	0.34	0.34	0.33	0.33	0.34	0.33	0.33
<b>Detection Rate</b>	0.21	0.12	0.32	0.14	0.00	0.26	0.21	0.02	0.27

<b>Detection Prevalence</b>	0.28	0.12	0.32	0.32	0.00	0.68	0.38	0.04	0.58
<b>Balanced Accuracy</b>	0.77	0.63	0.82	0.58	0.50	0.56	0.69	0.52	0.68

795 **Acknowledgements** This research was supported by funding from the InStream cohort and discussions with the participating scientists. Support to FS was provided by the Reduced Complexity Models project co-funded by the Helmholtz Association; and FS and RK acknowledge the Advanced Earth Modelling Capacity (ESM) project funded by the Helmholtz Association. We further thank Remi Dupas for providing French nitrate CQ data and Pia Ebeling for the German catchments characteristics data.

800

**Author contributions** JD and AM designed the study together with RK. JD developed the model code, carried out the simulations and interpreted them. FS provided help with the PAWN method. JD and AM prepared the manuscript draft and all co-authors contributed to reviewing and editing the manuscript.

805 **Competing interests** The authors declare that they have no conflict of interest.

## References

- Abbott, B. W., Gruau, G., Zarnetske, J. P., Moatar, F., Barbe, L., Thomas, Z., Fovet, O., Kolbe, T., Gu, S., Pierson-Wickmann, A. C., Davy, P., and Pinay, G.: Unexpected spatial stability of water chemistry in headwater stream networks, *Ecol Lett*, 21, 296-308, 10.1111/ele.12897, 2018.
- 810 Aguilera, R., Marcé, R., and Sabater, S.: Modeling nutrient retention at the watershed scale: Does small stream research apply to the whole river network?, *J Geophys Res-Biogeophys*, 118, 728-740, 10.1002/jgrg.20062, 2013.
- Alexander, R. B., Böhlke, J. K., Boyer, E. W., David, M. B., Harvey, J. W., Mulholland, P. J., Seitzinger, S. P., Tobias, C. R., Tonitto, C., and Wollheim, W. M.: Dynamic modeling of nitrogen losses in river networks unravels the coupled effects of hydrological and biogeochemical processes, *Biogeochemistry*, 93, 91-116, 10.1007/s10533-008-9274-8, 2009.
- 815 Alexander, R. B., Smith, R. A., and Schwarz, G. E.: Effect of stream channel size on the delivery of nitrogen to the Gulf of Mexico, *Nature*, 403, 758-761, 10.1038/35001562, 2000.
- Ameli, A. A., Beven, K., Erlandsson, M., Creed, I. F., McDonnell, J. J., and Bishop, K.: Primary weathering rates, water transit times, and concentration-discharge relations: A theoretical analysis for the critical zone, *Water Resour Res*, 53, 942-960, 10.1002/2016wr019448, 2017.
- 820 Andreadis, K. M., Schumann, G. J. P., and Pavelsky, T.: A simple global river bankfull width and depth database, *A simple global river bankfull width and depth database*, 49, 7164-7168, 10.1002/wrcr.20440, 2013.

- Basu, N. B., Rao, P. S. C., Thompson, S. E., Loukinova, N. V., Donner, S. D., Ye, S., and Sivapalan, M.: Spatiotemporal averaging of in-stream solute removal dynamics, *Water Resour Res*, 47, 10.1029/2010wr010196, 2011.
- 825 Bergstrom, A., McGlynn, B., Mallard, J., and Covino, T.: Watershed structural influences on the distributions of stream network water and solute travel times under baseflow conditions, *Hydrol Process*, 30, 2671-2685, 10.1002/hyp.10792, 2016.
- Bertuzzo, E., Helton, A. M., Hall, R. O., and Battin, T. J.: Scaling of dissolved organic carbon removal in river networks, *Adv Water Resour*, 110, 136-146, 10.1016/j.advwatres.2017.10.009, 2017.
- 830 Beusen, A. H. W., Bouwman, A. F., Van Beek, L. P. H., Mogollon, J. M., and Middelburg, J. J.: Global riverine N and P transport to ocean increased during the 20th century despite increased retention along the aquatic continuum, *Biogeosciences*, 13, 2441-2451, 10.5194/bg-13-2441-2016, 2016.
- Bieroza, M. Z., Heathwaite, A. L., Bechmann, M., Kyllmar, K., and Jordan, P.: The concentration-discharge slope as a tool for water quality management, *Sci Total Environ*, 630, 738-749, 10.1016/j.scitotenv.2018.02.256, 2018.
- Billen, G., Lancelot, C., and Meybeck, M.: N, P and Si retention along the aquatic continuum from land to ocean., N, P and Si retention along the aquatic continuum from land to ocean., 1 ed., 19-44, 1991.
- 835 Birgand, F., Skaggs, R. W., Chescheir, G. M., and Gilliam, J. W.: Nitrogen removal in streams of agricultural catchments - A literature review, *Crit Rev Env Sci Tec*, 37, 381-487, 10.1080/10643380600966426, 2007.
- Botter, G., Basso, S., Rodriguez-Iturbe, I., and Rinaldo, A.: Resilience of river flow regimes. *Proceedings of the National Academy of Sciences of the United States of America*, 110(32), 12925-12930, 10.1073/pnas.1311920110, 2013.
- 840 Bouwman, A. F., Bierkens, M. F. P., Griffioen, J., Hefting, M. M., Middelburg, J. J., Middelkoop, H., and Slomp, C. P.: Nutrient dynamics, transfer and retention along the aquatic continuum from land to ocean: towards integration of ecological and biogeochemical models, *Biogeosciences*, 9, 8733-8782, 10.5194/bgd-9-8733-2012, 2012.
- Boyer, E. W., Alexander, R. B., Parton, W. J., Li, C. S., Butterbach-Bahl, K., Donner, S. D., Skaggs, R. W., and Del Gross, S. J.: Modeling denitrification in terrestrial and aquatic ecosystems at regional scales, *Ecol Appl*, 16, 2123-2142, 10.1890/1051-0761(2006)016[2123:Mditaa]2.0.Co;2, 2006.
- 845 Breiman, L., Friedman, J., Stone, C. J., and Olshen, R. A.: *Classification and Regression Trees*, Chapman & Hall, London:, 1984.
- Canfield, D. E., Glazer, A. N., and Falkowski, P. G.: The evolution and future of Earth's nitrogen cycle, *Science*, 330, 192-196, 10.1126/science.1186120, 2010.
- Diamond, J. S. and Cohen, M. J.: Complex patterns of catchment solute-discharge relationships for coastal plain rivers, *Hydrol Process*, 32, 388-401, 10.1002/hyp.11424, 2018.
- 850 Dingman, S. L.: Analytical derivation of at-a-station hydraulic-geometry relations, *J Hydrol*, 334, 17-27, 10.1016/j.jhydrol.2006.09.021, 2007.
- Doyle, M. W.: Incorporating hydrologic variability into nutrient spiraling, *J Geophys Res*, 110, 10.1029/2005jg000015, 2005.
- Dupas, R., Minaudo, C., and Abbott, B. W.: Stability of spatial patterns in water chemistry across temperate ecoregions, 855 *Environ Res Lett*, 14, 10.1088/1748-9326/ab24f4, 2019.

- Dupas, R., Musolff, A., Jawitz, J., Rao, P. S. C., Jager, C. G., Fleckenstein, J. H., Rode, M., and Borchardt, D.: Carbon and nutrient export regimes from headwater catchments to downstream reaches, *Biogeosciences*, 14, 4391-4407, 10.5194/bg-14-4391-2017, 2017.
- Durand, P., Breuer, L., Johnes, P. J., Billen, G., Butturini, A., Pinay, G., and Wright, R.: Nitrogen processes in aquatic ecosystems. In: *The European Nitrogen Assessment: Sources, Effects and Policy Perspectives*, Sutton, M., Howard, C., Erisman, J., Billen, G., Bleeker, A., Grennfelt, P., and al., e. (Eds.), Cambridge University Press, Cambridge, 2011.
- Ebeling, P.: CCDB - catchment characteristics data base Germany. HydroShare, 2020a.
- Ebeling, P.: WQQDB - water quality metrics for catchments across Germany HydroShare, 2020b.
- Ebeling, P., Kumar, R., Weber, M., Knoll, L., Fleckenstein, J. H., and Musolff, A.: Archetypes and Controls of Riverine Nutrient Export Across German Catchments, *Water Resour Res*, 10.1029/2020WR028134, 2021.
- EEA: DEM over Europe from the GMES RDA project (EU-DEM, resolution 25m) - version 1, Oct. 2013, edited, European Environmental Agency, 2013.
- Ehrhardt, S., Kumar, R., Fleckenstein, J. H., Attinger, S., and Musolff, A.: Trajectories of nitrate input and output in three nested catchments along a land use gradient, *Hydrol Earth Syst Sc*, 23, 3503-3524, 10.5194/hess-23-3503-2019, 2019.
- Ensign, S. H. and Doyle, M. W.: Nutrient spiraling in streams and river networks, *J Geophys Res-Biogeophys*, 111, 10.1029/2005jg000114, 2006.
- Ensign, S. H., McMillan, S. K., Thompson, S. P., and Piehler, M. F.: Nitrogen and phosphorus attenuation within the stream network of a coastal, agricultural watershed, *J Environ Qual*, 35, 1237-1247, 10.2134/jeq2005.0341, 2006.
- ESRI: ArcGIS Desktop: Release 10. Redlands, CA: Environmental Systems Research Institute., 2011.
- Fisher, S. G., Sponseller, R. A., and Heffernan, J. B.: Horizons in stream biogeochemistry: Flowpaths to progress, *Ecology*, 85, 2369-2379, 10.1890/03-0244, 2004.
- Galloway, J. N., Schlesinger, W. H., Levy, H., Michaels, A., and Schnoor, J. L.: Nitrogen fixation: Anthropogenic enhancement-environmental response, *Global Biogeochem Cy*, 9, 235-252, 10.1029/95gb00158, 1995.
- Godsey, S. E., Kirchner, J. W., and Clow, D. W.: Concentration-discharge relationships reflect chemostatic characteristics of US catchments, *Hydrol Process*, 23, 1844-1864, 10.1002/hyp.7315, 2009.
- Gomez-Velez, J. D., Harvey, J., Cardenas, M. B., and Kiel, B.: Denitrification in the Mississippi River network controlled by flow through river bedforms, *Nat Geosci*, 8, 941-U975, 10.1038/Ngeo2567, 2015.
- Hall, R. O., Tank, J. L., Sobota, D. J., and Mulholland, P. J.: Nitrate removal in stream ecosystems measured by <sup>15</sup>N addition experiments: Total uptake, *Limnol Oceanogr*, 54, 653-665, 10.4319/lo.2009.54.3.0653, 2009.
- Helton, A. M., Hall, R. O., and Bertuzzo, E.: How network structure can affect nitrogen removal by streams, *Freshwater Biol*, 63, 128-140, 10.1111/fwb.12990, 2018.
- Helton, A. M., Poole, G. C., Meyer, J. L., Wollheim, W. M., Peterson, B. J., Mulholland, P. J., Bernhardt, E. S., Stanford, J. A., Arango, C., Ashkenas, L. R., Cooper, L. W., Dodds, W. K., Gregory, S. V., Hall, R. O., Hamilton, S. K., Johnson, S. L.,



- McDowell, W. H., Potter, J. D., Tank, J. L., Thomas, S. M., Valett, H. M., Webster, J. R., and Zeglin, L.: Thinking outside the channel: modeling nitrogen cycling in networked river ecosystems, *Front Ecol Environ*, 9, 229-238, 10.1890/080211, 2010.
- 890 Hensley, R. T., Cohen, M. J., and Korhnak, L. V.: Inferring nitrogen removal in large rivers from high-resolution longitudinal profiling, *Limnol Oceanogr*, 59, 1152-1170, 10.4319/lo.2014.59.4.1152, 2014.
- Horton, R. E.: Erosional Development of Streams and Their Drainage Basins - Hydrophysical Approach to Quantitative Morphology, *Geol Soc Am Bull*, 56, 275-370, 10.1130/0016-7606(1945)56[275:edosat]2.0.co;2, 1945.
- 895 Jarvie, H. P., Sharpley, A. N., Kresse, T., Hays, P. D., Williams, R. J., King, S. M., and Berry, L. G.: Coupling High-Frequency Stream Metabolism and Nutrient Monitoring to Explore Biogeochemical Controls on Downstream Nitrate Delivery, *Environ Sci Technol*, 52, 13708-13717, 10.1021/acs.est.8b03074, 2018.
- Jawitz, J. W. and Mitchell, J.: Temporal inequality in catchment discharge and solute export, *Water Resour Res*, 47, 10.1029/2010wr010197, 2011.
- 900 Kadlec, R. H. and Reddy, K. R.: Temperature effects in treatment wetlands, *Water Environ Res*, 73, 543-557, 10.2175/106143001x139614, 2001.
- Kiel, B. A. and Cardenas, M. B.: Lateral hyporheic exchange throughout the Mississippi River network, *Nat Geosci*, 7, 413-417, 10.1038/Ngeo2157, 2014.
- Kirchner, J. W., Feng, X., and Neal, C.: Fractal stream chemistry and its implications for contaminant transport in catchments, 905 *Nature*, 403, 524-527, 10.1038/35000537, 2000.
- Klemes, V.: Dilettantism in Hydrology - Transition or Destiny, *Water Resour Res*, 22, S177-S188, 10.1029/WR022i09Sp0177S, 1986.
- Kuhn, M.: caret: Classification and Regression Training. 2020.
- Kumar, R., Hesse, F., Rao, P. S. C., Musolff, A., Jawitz, J. W., Sarrazin, F., Samaniego, L., Fleckenstein, J. H., Rakovec, O., 910 Thober, S., and Attinger, S.: Strong hydroclimatic controls on vulnerability to subsurface nitrate contamination across Europe, *Nat Commun*, 11, 6302, 10.1038/s41467-020-19955-8, 2020.
- Kunz, J. V., Hensley, R., Brase, L., Borchardt, D., and Rode, M.: High frequency measurements of reach scale nitrogen uptake in a fourth order river with contrasting hydromorphology and variable water chemistry (Weisse Elster, Germany), *Water Resour Res*, 53, 328-343, 10.1002/2016wr019355, 2017.
- 915 Langbein, W. B. and Leopold, L. B.: Quasi-Equilibrium States in Channel Morphology, *Am J Sci*, 262, 782-&, 10.2475/ajs.262.6.782, 1964.
- Leopold, L. B. and Maddock, T.: The hydraulic geometry of stream channels and some physiographic implications, Washington, D.C., 1953.
- Li, L., Sullivan, P. L., Benettin, P., Cirpka, O. A., Bishop, K., Brantley, S. L., Knapp, J. L. A., Meerveld, I., Rinaldo, A., 920 Seibert, J., Wen, H., and Kirchner, J. W.: Toward catchment hydro-biogeochemical theories, *WIREs Water*, 8, 10.1002/wat2.1495, 2020.

- Lindgren, G. A. and Destouni, G.: Nitrogen loss rates in streams: Scale-dependence and up-scaling methodology, *Geophys Res Lett*, 31, 1-4, 10.1029/2004gl019996, 2004.
- Marce, R. and Armengol, J.: Modeling nutrient in-stream processes at the watershed scale using Nutrient Spiralling metrics, 925 *Hydrol Earth Syst Sc*, 13, 953-967, 10.5194/hess-13-953-2009, 2009.
- Marcé, R., von Schiller, D., Aguilera, R., Martí, E., and Bernal, S.: Contribution of Hydrologic Opportunity and Biogeochemical Reactivity to the Variability of Nutrient Retention in River Networks, *Global Biogeochem Cy*, 32, 376-388, 10.1002/2017gb005677, 2018.
- Marinos, R. E., Van Meter, K. J., and Basu, N. B.: Is the River a Chemostat?: Scale Versus Land Use Controls on Nitrate 930 Concentration-Discharge Dynamics in the Upper Mississippi River Basin, *Geophys Res Lett*, 47, 10.1029/2020gl087051, 2020.
- McDonnell, J. J., Sivapalan, M., Vaché, K., Dunn, S., Grant, G., Haggerty, R., Hinz, C., Hooper, R., Kirchner, J., Roderick, M. L., Selker, J., and Weiler, M.: Moving beyond heterogeneity and process complexity: A new vision for watershed hydrology, *Water Resour Res*, 43, 10.1029/2006wr005467, 2007.
- 935 Meybeck, M. and Moatar, F.: Daily variability of river concentrations and fluxes: indicators based on the segmentation of the rating curve, *Hydrol Process*, 26, 1188-1207, 10.1002/hyp.8211, 2012.
- Minaudo, C., Dupas, R., Gascuel-Oudou, C., Roubeix, V., Danis, P.-A., and Moatar, F.: Seasonal and event-based concentration-discharge relationships to identify catchment controls on nutrient export regimes, *Adv Water Resour*, 131, 10.1016/j.advwatres.2019.103379, 2019.
- 940 Mineau, M. M., Wollheim, W. M., and Stewart, R. J.: An index to characterize the spatial distribution of land use within watersheds and implications for river network nutrient removal and export, *Geophys Res Lett*, 42, 6688-6695, 10.1002/2015gl064965, 2015.
- Moatar, F., Abbott, B. W., Minaudo, C., Curie, F., and Pinay, G.: Elemental properties, hydrology, and biology interact to shape concentration-discharge curves for carbon, nutrients, sediment, and major ions, *Water Resour Res*, 53, 1270-1287, 945 10.1002/2016wr019635, 2017.
- Mueller, C., Musolff, A., Strachauer, U., Brauns, M., Tarasova, L., Merz, R., and Knöller, K.: Tomography of anthropogenic nitrate contribution along a mesoscale river, *Sci Total Environ*, 615, 773-783, 10.1016/j.scitotenv.2017.09.297, 2018.
- Mulholland, P. J., Helton, A. M., Poole, G. C., Hall, R. O., Hamilton, S. K., Peterson, B. J., Tank, J. L., Ashkenas, L. R., Cooper, L. W., Dahm, C. N., Dodds, W. K., Findlay, S. E., Gregory, S. V., Grimm, N. B., Johnson, S. L., McDowell, W. H., 950 Meyer, J. L., Valett, H. M., Webster, J. R., Arango, C. P., Beaulieu, J. J., Bernot, M. J., Burgin, A. J., Crenshaw, C. L., Johnson, L. T., Niederlehner, B. R., O'Brien, J. M., Potter, J. D., Sheibley, R. W., Sobota, D. J., and Thomas, S. M.: Stream denitrification across biomes and its response to anthropogenic nitrate loading, *Nature*, 452, 202-205, 10.1038/nature06686, 2008.
- Mulholland, P. J. and Tank, J. L.: Can uptake length in streams be determined by nutrient addition experiments? Results from 955 an interbiome comparison study, *J N Am Benthol Soc*, 21, 544-560, 10.2307/1468429, 2002.

- Musolff, A.: WQQDB - water quality and quantity data base Germany: metadata. Hydroshare, 2020.
- Musolff, A., Fleckenstein, J. H., Rao, P. S. C., and Jawitz, J. W.: Emergent archetype patterns of coupled hydrologic and biogeochemical responses in catchments, *Geophys Res Lett*, 44, 4143-4151, 10.1002/2017gl072630, 2017.
- Newbold, J. D., Elwood, J. W., Oneill, R. V., and Vanwinkle, W.: Measuring Nutrient Spiralling in Streams, *Can J Fish Aquat Sci*, 38, 860-863, DOI 10.1139/f81-114, 1981.
- O'Brien, J. M., Dodds, W. K., Wilson, K. C., Murdock, J. N., and Eichmiller, J.: The saturation of N cycling in Central Plains streams: 15N experiments across a broad gradient of nitrate concentrations, *Biogeochemistry*, 84, 31-49, 10.1007/s10533-007-9073-7, 2007.
- Ocampo, C. J., Oldham, C. E., and Sivapalan, M.: Nitrate attenuation in agricultural catchments: Shifting balances between transport and reaction, *Water Resour Res*, 42, 10.1029/2004wr003773, 2006.
- Oldham, C. E., Farrow, D. E., and Peiffer, S.: A generalized Damköhler number for classifying material processing in hydrological systems, *Hydrol Earth Syst Sc*, 17, 1133-1148, 10.5194/hess-17-1133-2013, 2013.
- Pennino, M. J., Kaushal, S. S., Beaulieu, J. J., Mayer, P. M., and Arango, C. P.: Effects of urban stream burial on nitrogen uptake and ecosystem metabolism: implications for watershed nitrogen and carbon fluxes, *Biogeochemistry*, 121, 247-269, 10.1007/s10533-014-9958-1, 2014.
- Peterson, B. J., Wollheim, W. M., Mulholland, P. J., Webster, J. R., Meyer, J. L., Tank, J. L., Marti, E., Bowden, W. B., Valett, H. M., Hershey, A. E., McDowell, W. H., Dodds, W. K., Hamilton, S. K., Gregory, S., and Morrall, D. D.: Control of nitrogen export from watersheds by headwater streams, *Science*, 292, 86-90, 10.1126/science.1056874, 2001.
- Pianosi, F., Sarrazin, F., and Wagener, T.: A Matlab toolbox for Global Sensitivity Analysis, *Environ Modell Softw*, 70, 80-85, 10.1016/j.envsoft.2015.04.009, 2015.
- Pianosi, F. and Wagener, T.: Distribution-based sensitivity analysis from a generic input-output sample, *Environ Modell Softw*, 108, 197-207, 10.1016/j.envsoft.2018.07.019, 2018.
- Pianosi, F. and Wagener, T.: A simple and efficient method for global sensitivity analysis based on cumulative distribution functions, *Environ Modell Softw*, 67, 1-11, 10.1016/j.envsoft.2015.01.004, 2015.
- Pinay, G., Peiffer, S., De Dreuzy, J. R., Krause, S., Hannah, D. M., Fleckenstein, J. H., Sebilo, M., Bishop, K., and Hubert-Moy, L.: Upscaling Nitrogen Removal Capacity from Local Hotspots to Low Stream Orders' Drainage Basins, *Ecosystems*, 18, 1101-1120, 10.1007/s10021-015-9878-5, 2015.
- Pressley, A. N.: *Elementary Differential Geometry* (1<sup>st</sup> ed.), 10.1007/978-1-84882-891-9, 2001.
- R Core Team: *R: A language and environment for statistical computing*. R Foundation for Statistical Computing, Vienna, Austria, 2013.
- Risse-Buhl, U., Anlanger, C., Kalla, K., Neu, T. R., Noss, C., Lorke, A., and Weitere, M.: The role of hydrodynamics in shaping the composition and architecture of epilithic biofilms in fluvial ecosystems, *Water Res*, 127, 211-222, 10.1016/j.watres.2017.09.054, 2017.

- Rode, M., Halbedel Nee Angelstein, S., Anis, M. R., Borchardt, D., and Weitere, M.: Continuous In-Stream Assimilatory Nitrate Uptake from High-Frequency Sensor Measurements, *Environ Sci Technol*, 50, 5685-5694, 10.1021/acs.est.6b00943, 2016.
- Runkel, R. L. and Bencala, K. E.: Transport of reacting solutes in rivers and streams. In: *Environmental Hydrology, Water Science and Technology Library*, 1995.
- Schlesinger, W. H., Reckhow, K. H., and Bernhardt, E. S.: Global change: The nitrogen cycle and rivers, *Water Resour Res*, 42, 10.1029/2005wr004300, 2006.
- Seitzinger, S. P., Styles, R. V., Boyer, E. W., Alexander, R. B., Billen, G., Howarth, R. W., Mayer, B., and Van Breemen, N.: Nitrogen retention in rivers: model development and application to watersheds in the northeastern U.S.A., *Biogeochemistry*, 57/58, 199–237, 10.1023/A:1015745629794, 2002.
- Seybold, E. and McGlynn, B.: Hydrologic and biogeochemical drivers of dissolved organic carbon and nitrate uptake in a headwater stream network, *Biogeochemistry*, 138, 23-48, 10.1007/s10533-018-0426-1, 2018.
- Stream Solute Workshop: Concepts and Methods for Assessing Solute Dynamics in Stream Ecosystems, *J N Am Benthol Soc*, 9, 95-119, 10.2307/1467445, 1990.
- Tunqui Neira, J. M., Andréassian, V., Tallec, G., and Mouchel, J.-M.: Technical note: A two-sided affine power scaling relationship to represent the concentration–discharge relationship, *Hydrol. Earth Syst. Sci.*, 24, 1823–1830, 10.5194/hess-24-1823-2020, 2020.
- Vanni, M. J.: Nutrient Cycling by Animals in Freshwater Ecosystems, *Nutrient Cycling by Animals in Freshwater Ecosystems*, 33, 341-370, 10.1146/annurev.ecolsys.33.010802.150519, 2002.
- Vanni, M. J. and McIntyre, P. B.: Predicting nutrient excretion of aquatic animals with metabolic ecology and ecological stoichiometry: a global synthesis, *Ecology*, 97, 3460-3471, 10.1002/ecy.1582, 2016.
- Wei, T. and Simko, V.: R package "corrplot": Visualization of a Correlation Matrix 2020.
- Winter, C., Lutz, S. R., Musolff, A., Kumar, R., Weber, M., and Fleckenstein, J. H.: Disentangling the impact of catchment heterogeneity on nitrate export dynamics from event to long-term time scales, *Water Resour Res*, doi: 10.1002/essoar.10503228.1, 2020. 10.1002/essoar.10503228.1, 2020.
- Wollheim, W. M., Bernal, S., Burns, D. A., Czuba, J. A., Driscoll, C. T., Hansen, A. T., Hensley, R. T., Hosen, J. D., Inamdar, S., Kaushal, S. S., Koenig, L. E., Lu, Y. H., Marzadri, A., Raymond, P. A., Scott, D., Stewart, R. J., Vidon, P. G., and Wohl, E.: River network saturation concept: factors influencing the balance of biogeochemical supply and demand of river networks, *Biogeochemistry*, 141, 503-521, 10.1007/s10533-018-0488-0, 2018.
- Wollheim, W. M., Mulukutla, G. K., Cook, C., and Carey, R. O.: Aquatic Nitrate Retention at River Network Scales Across Flow Conditions Determined Using Nested In Situ Sensors, *Water Resour Res*, 53, 9740-9756, 10.1002/2017wr020644, 2017.
- Wollheim, W. M., Peterson, B. J., Thomas, S. M., Hopkinson, C. H., and Vörösmarty, C. J.: Dynamics of N removal over annual time periods in a suburban river network, *J Geophys Res*, 113, 10.1029/2007jg000660, 2008.

Wollheim, W. M., Vörösmarty, C. J., Peterson, B. J., Seitzinger, S. P., and Hopkinson, C. S.: Relationship between river size and nutrient removal, *Geophys Res Lett*, 33, 10.1029/2006gl025845, 2006.

1025 Yang, X., Jomaa, S., Buttner, O., and Rode, M.: Autotrophic nitrate uptake in river networks: A modeling approach using continuous high-frequency data, *Water Res*, 157, 258-268, 10.1016/j.watres.2019.02.059, 2019.

Yang, X. Q., Jomaa, S., Zink, M., Fleckenstein, J. H., Borchardt, D., and Rode, M.: A New Fully Distributed Model of Nitrate Transport and Removal at Catchment Scale, *Water Resour Res*, 54, 5856-5877, 10.1029/2017wr022380, 2018.

Zarnetske, J. P., Haggerty, R., Wondzell, S. M., and Baker, M. A.: Dynamics of nitrate production and removal as a function of residence time in the hyporheic zone, *J Geophys Res*, 116, 10.1029/2010jg001356, 2011.